12-2021

Analysis of Bacteriorhodopsin Suspended in a Bilayer Lipid Membrane

Moath Alhejji
University of Arkansas, Fayetteville

Analysis of Bacteriorhodopsin Suspended in a Bilayer Lipid Membrane

A thesis submitted in partial fulfillment
of the requirements for the degree of
Master of Science in Physics

by

Moath Alhejji
King Saud University
Bachelor of Science in Physics, 2015

December 2021
University of Arkansas

This thesis is approved for recommendation to the Graduate Council.

Jiali Li, Ph.D.
Thesis Director

Hamed Naseem, Ph.D.
Committee Member

Pradeep Kumar, Ph.D.
Committee Member

Abstract

The bacteriorhodopsin protein's unique characteristic of proton pumping can convert light energy to electric energy. The aim of this research was to generate photocurrent using bacteriorhodopsin in a bi-layer lipid membrane. Lipid monolayer and bilayer were formed using painting and folding methods, respectively. Capacitance and resistance of the lipid membranes were measured and used to validate the best methodology. My results show that the folding method is more efficient in incorporating Bacteriorhodopsin. The photocurrent was generated by illuminating a green laser (532 nm) on the bilayer lipid membranes. The patch clamp electrophysiology technique was used to apply voltage across the lipid membrane and to record photocurrent. For the membrane capacitance and resistance, the ranges were ($1.70E^{-01}$- $7.50E^{-01}$ uF/cm^2) and (0.30 - 0.49 GΩ), respectively. The photocurrent density produced was between 5.3 pA/cm^2 and 7.1 pA/cm^2.

Acknowledgment

First, I would like to express my deepest appreciation to my advisor, Dr. Jiali Li, for providing great consultations and continuous motivation to make this work done. Also, I would like to thank Dr. Li's lab group members Mitu Acharjee and Joel Kamwa from whom I learned different aspects of research.

Also, I would like to thank my close friends Sean Cannon, Kaite Cannon, and Bethany Peevy who never made me feel that I was a stranger since coming to the US. Their support was a source of strength especially when life rhythm goes down. Without them, this work would not be what it is.

Finally, I would like to thank my family who lives far away in another part of this world, but their unconditional emotional support always makes me feel that they are close to me.

Table of contents

List of Figures

Chapter 1: Introduction

The motivation of this Work

In the past, fossil fuels were predominantly as means of energy. However, due to negative environmental impacts of fossil fuels led to search for alternate efficient energy sources without negative side effects. The discovery of renewable energy sources has led to reducing fossil fuel use. The popularity of using renewable energy sources has inspired scientists to find solutions that can contribute to making the environment healthier. One of the most promising techniques to convert sunlight into photocurrent is using a proton-pumping system such as bacteriorhodopsin reconstituted in a bi-layer membrane. Hence, this work aims to investigate bacteriorhodopsin (bR), a photosynthetic protein, to generate the photocurrent.

Chapter 2: Bacteriorhodopsin

2.1 Definition

There are some photosynthetic proteins capable of converting light into photocurrent, and these types of proteins have a common structure called rhodopsin. Rhodopsin is also known as a chromoprotein which is a Greek word meaning color [1]. Bacteriorhodopsin is a photosynthetic protein found in *Halobacterium salinarum (H. salinarum)* that was discovered in 1966 and its ability to act as a light-driven proton pump was identified in 1972 [2]. A cartoon representation of a monomer of bR is shown in Fig. 2.1. The bR protein is comprised of 248 amino acids and the molecular weight is 26 KDa. bR trimers form a two-dimensional hexagonal structure in the membrane of *H. salinarum*.

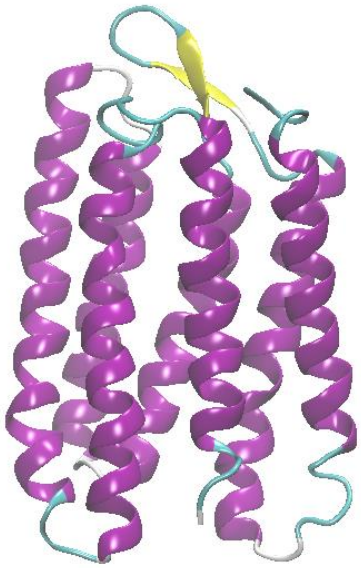

Figure 2.1. Bacteriorhodopsin from *Halobacterium Salinarum* [3].

It has been found that two major environmental factors are attributed to the expression of bR protein in *H. salinarum* —(i) low oxygen pressure, and (ii) light [4]. Furthermore, it was shown that the membrane from *Halobacterium salinarum,* also called purple membrane due to its distinguished color [6], is comprised of 25 % lipid and 75% protein by weight.

Photophosphorylation mechanism is used to convert light energy that strikes *H. salinarum* into chemical energy in the form of ATP [5] as illustrated in Fig. 2.2. The wavelength of light required to actively transport a proton outside the cell is 400-600 nm that generates a proton gradient and ATP production. A proton gradient is formed due to the translocation of protons from the cytoplasmic to the extracellular side of the phospholipid bilayers.

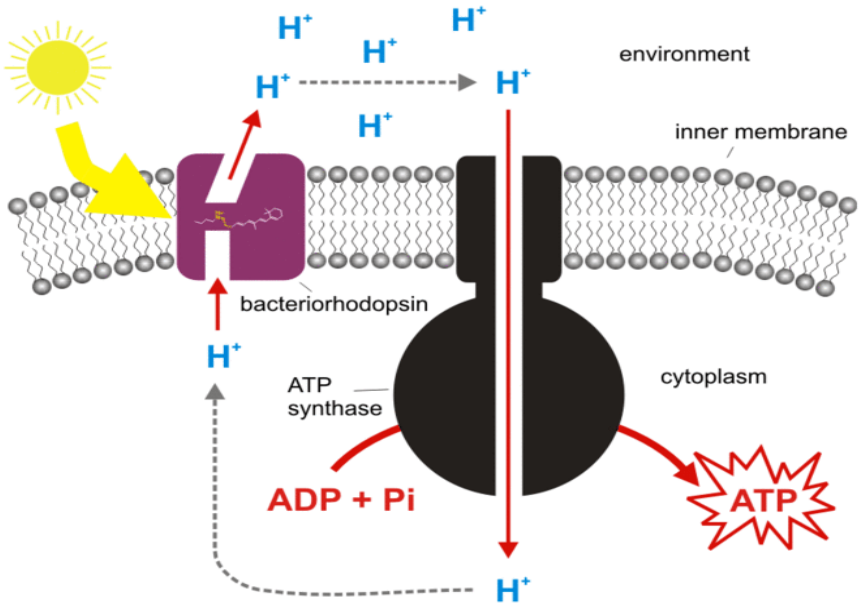

Figure 2.2 ATP generated due to the presence of bacteriorhodopsin [5]

bR protein has also been used in generating photocurrent due to its proton pumping ability. Because of its very high thermal stability and capability to remain biologically active for many years, bR is an ideal source of renewable energy [7]. In addition, the photocurrent can be directed in one direction by applying external voltage across the membrane. The produced photovoltage can be identified by its bipolarity starting from a negative spike estimated (ps) followed by a positive spike estimated (µs to ms) [8]**.** However, in some situations, bR protein can function its own as current-carrying based on the devices used [9].

2.2 History and Theory (working principle)

In addition, recent investigation of *Halobacterium halobium* suggest that bacteriorhodopsin (bR) and halorhodopsin (hR) are the two proteins that can induce an electrochemical gradient when incorporated into lipid membranes [2]. This part is dedicated to highlighting the structure and the mechanism of the bR protein by mentioning the recent applications of the bR protein.

In 1975, under low resolution, electron crystallography was used to identify the structure of bR that consists of seven alpha-helical segments. The retinal is a small molecule which is responsible to absorb visible light. Since it is sensitive to very low levels of light, it causes an ongoing twist for the retinal. That results in release of protons. Although a lack of information existed about the retinal, it was highly expected to be found in the hydrophobic interior of the cluster. Retinal large redshift and the increases of the chromophore acid dissociation constant (pK) are attributed to the change of bR structure [2].

In 1976, 280 mV was the highest voltage measured by Michel and Oesterhelt that bacteriorhodopsin from *Halobacterium halobium* can generate [10]. Scientists have put a large effort into analyzing the structure of bR because knowing the structure paves the road for scientists to accurately study how the protons' path behaves when light strikes the bR protein. In general, the structure of bR is comprised of seven helices, which are named with letters A, B, C, D, E, F, and G, and surround a retinal chromophore, which includes the proton channel. The channel spans from cytoplasmic to extracellular region. The Schiff base, which plays a significant role in donating protons from the extracellular to the cytoplasmic regions, is located at the center of these channels specifically in helix G connected to lysine 216 [11]. Electron microscopy was used to identify and the map structure of bR [12]. Later, high resolution

structure of bR have been obtained due to the rapid progress of advanced devices. For example, Hasegawa et al. (2018) showed that the highest resolution recorded for the bR structure is 1.3A offering the capability of observing the individual atoms of the residues by using x-ray analysis [13].

The bR working principle is based on the transfer of protons from the extracellular to the cytoplasmic side within a catalytic cycle. More specifically, the catalytic cycle starts when the bR absorbs a photon (light) and leads to the transport of one proton from an amino acid called "Asparate" Asp85 (proton acceptor) to Asp96 (proton donor). Nevertheless, the transfer of the proton will not happen without a connection between a proton acceptor and a proton donor. Kandori (2000) explained that there are two necessary conditions required to achieve proton pumping: creating a pathway and switching machinery. In the presence of water molecules, the translocations of protons through the hydrophilic region can be achieved by forming a hydrogen – bonding network. Therefore, pumping of protons from one side to another side of membrane requires water molecules to carry protons. FTIR spectroscopy has been used to monitor the change in the bR structure in the presence of water molecules during the proton pumping process [14]. Because of the transport of protons from the cytoplasmic side to the extracellular side, the photon isomerizes the retinal, and the isomerization of the retinal causes conformational changes. Stoeckenius [3] found that the changes of the retinal occurred during the first part of photocycle, known as the proton transport from K to M1, are small compared to the huge changes of the retinal for the second part of photocycle, known as the proton transport from M2 to O [3].

In general, the photocycle of bR can be formally described in terms of six phases called K, L, M1, M2, N, and O) distinguished by their spectroscopic fingerprints based on the ongoing isomerization of the bR retinal as shown in Figure 2.2. bR structure at each stage of the transfer

of the proton can be accurately identified by using x-ray diffraction, which has allowed scientists to analyze the mechanism of proton pumping within bR protein [16]**.** Between the K and L phase, the transfer of the first proton occurs from the Schiff base to Asp-85 since the hydrogen bonds interact with the proton acceptor Asp-85. After the intermediate states K, and L, the first proton translocation happens between two phases M_1 and M_2. The changes that happen between M_1, M_2, also called conformational changes in the retina, are responsible for the transition. Due to these significant changes at the end of the cytoplasmic part of the photocycle, that created a pathway for a proton to access the extracellular half channel through the H-bonded network. There is still debate about when deprotonation and protonation occur in the cytoplasmic part of the photocycle. In L phase, protonation of Schiff base and deprotonation of Asp-85 occur, while in M1 phase, the task is switched [15]. The proton will be absorbed from the cytoplasmic side during the N-O transition and the transitions from the O state back to the initial bR can take place. In this phase, the Schiff base gets reprotonated by Asp-96 which is known for its high pK value. Following, the restoration of Asp96 is achieved by the proton taken up from the cytoplasmic side. The phase that coincides with the uptake of proton is the Q phase. The estimated time of proton movements between M2 and the bR ground state is just milliseconds [17]. Wang, Facciotti, and Duan (2013) summarized the photocycle of the bR protein into three major processes called Isomerization of the retinal, Transfer of proton, and a Switch (ITS) in orientation from EC to IC [18]**.**

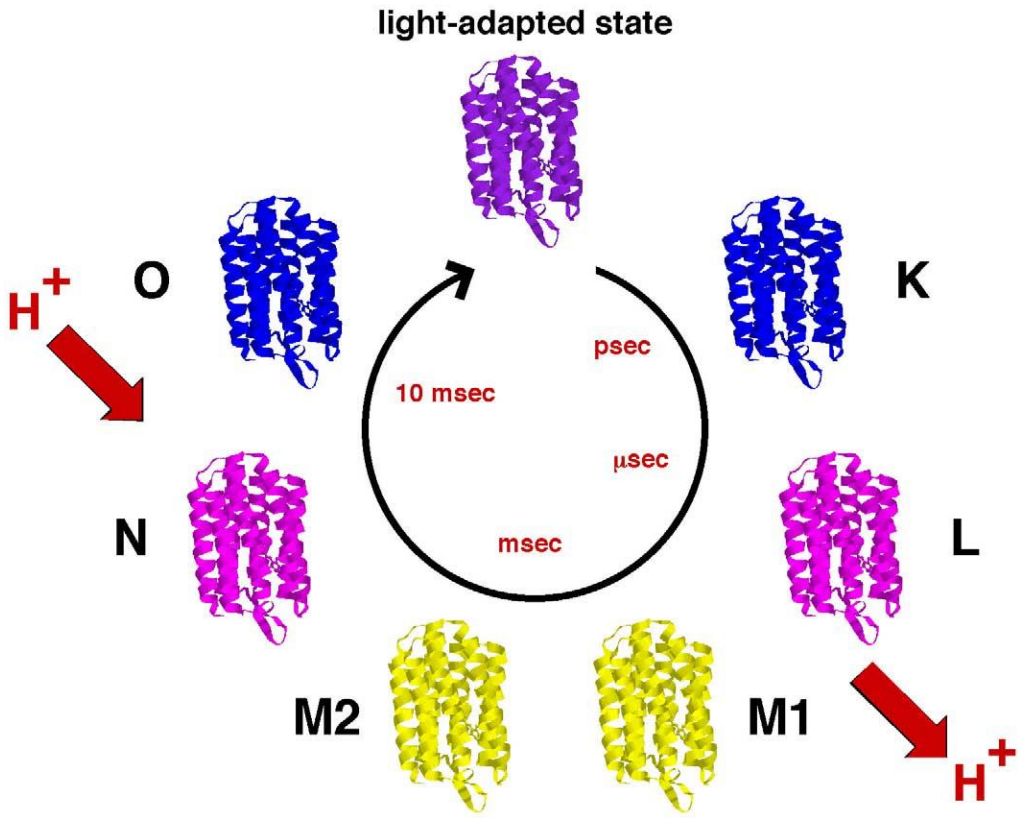

Figure 2.3 The photocycle of the bR protein [15].

The mechanism of deprotonation and reprotonation of the Schiff base from different sides of a membrane has been a separate major topic due to the changes accompanied by a proton transfer, specifically, during the two phases M1 and M2. Recent works have shed light on how the mechanism of the switch looks like after a primary proton transfer. More specifically, the question asked was why the accessibility of the Schiff base to the extracellular side of the membrane is impossible after the first primary proton transfer to Asp85. It has been found that structural changes are the main reason that do not allow the reverse proton transfer from Asp85 to the Schiff base. Besides structural changes, electrostatic effects contribute to increasing the barrier for reverse proton transfer between the Schiff base and Asp85, which makes the reprotonation of the Schiff base from Asp96 occur continuously [19]. The close distance between

the Schiff base and Asp85 makes the transfer of a proton from the Schiff base and Asp85 faster, compared to the long distance between Schiff base (SB) and Asp96. Also, the proton affinity (microstate energy) of Asp 85 and 96 has an obvious impact on the mechanism within the bR protein. To illustrate, due to the high proton affinity of Asp85, the reprotonation for Asp85 becomes difficult while in another side of the cell, Asp96 has a low proton affinity which allows for a proton easily to reprotonate SB from the cytoplasmic [20].

Furthermore, the effect of pH on proton transport has provides valuable insight into knowing when proton is released and reuptaken during the photocycle. Zimányi and others have found that the release of a proton between M1 and M2 and the reuptake of a proton in the transition N→O occur if pH >pKa. However, if pH <pKa, the reuptake of a proton in the transition N→O happens before the proton becomes released during the O→ BR transition [21].

Figure 2.4(a) illustrates the changes that happen in the retinal structure in the presence of visible light due to the transfer of a proton from the cytoplasmic side (IC) to the extracellular side (EC) of the membrane, causing retinal isomerization. The proton path is comprised of a group of charge residues such as Asp85 Asp212, and Tyr57 and water molecules necessary for efficient pumping activity in archaeal proton pumps [22]. Asp85 has two major functions: acceptor of the proton from the protonated SB and in the ground state, counterion to the SB2 [23].

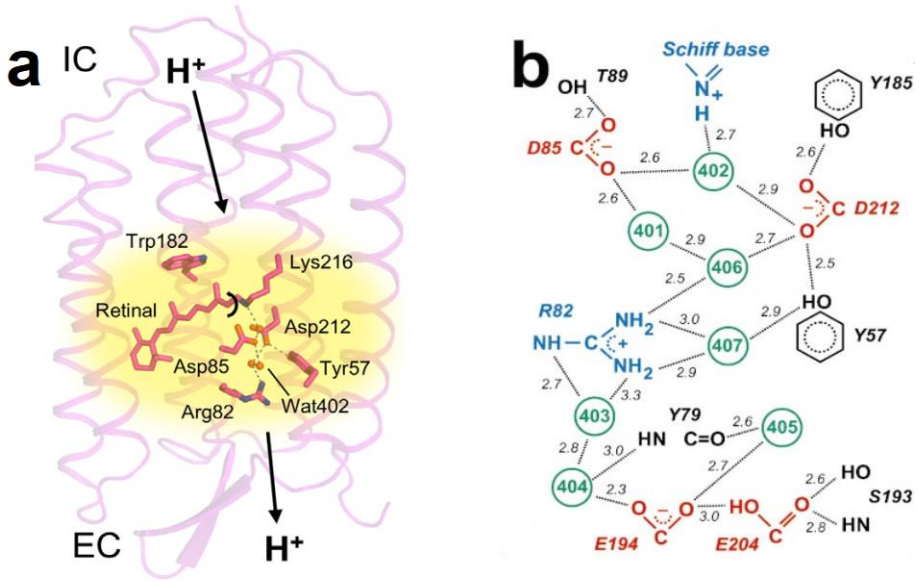

Figure 2.4 (a) The transfer of proton inside bacteriorhodopsin [22]. (b) Map of the hydrogen bonds [24].

Figure 2.4 (b) illustrates the structure of the hydrogen bond network which explains how the proton behaves starting from the Schiff base where the proton transfer originates. The release of a proton starts from the cytoplasmic side of the membrane to the extracellular surface (S193) via the E204 protonation.

The capability of the protein's ion pump reconstituted into lipid membranes and knowing and testing how the ions respond provides information on how to choose the appropriate quantity of lipid that makes ions transfer easier. For this reason, in this experiment, measuring membrane capacitance and resistance is an important along with other sequential steps.

2.3 Applications

The advantage of utilizing bacteriorhodopsin is not restricted only to a specific area. To

clarify, bR protein has been used in various applications. However, the most common field in which bR protein has been used is generating electrical signals due to its proton pumping ability. Besides its capability of proton pumping, there are many attributes of bR protein that have made bR an ideal source of alternative solar energy conversion. For example, its unique mechanism has drawn considerable attention by the continuation of photoconversion without losing its photonic properties [7]**.** Additionally, it can absorb a wide range of wavelengths of light compared to artificial sources such as N3 Dye; the absorption intensity of the bR protein molecules is double the value of artificial N3 dye. For a comparison, absorption spectra for the same concentration of N3 dye and bR protein (30 μM) are shown in figure 2.5 [25]**.**

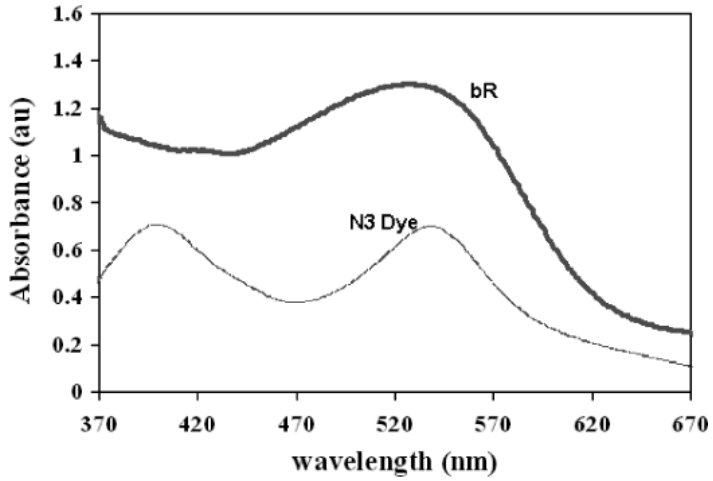

Figure 2.5 absorption spectrum bR and N3 Dye [25]

2.3.1 Biomolecule-sensitized solar cells (BSSCs)

After the invention of dye sensitized solar cells (DSSC) by Gratzel, scientists wondered if there was an alternate solution to substituting artificial dyes due to the toxicity and high costs of these dyes. The Characteristics of bR molecules have made this natural source an active zone of research for applications in bio sensitized solar cells (BSSC). Figure 2.7(b) shows the

structure of a BSSC made of bR molecules, nanostructure materials such as TiO_2 with a coated layer, an electrolyte, and counter electrode. Since the residues of the bR protein bear positive charge, it the binds to the TiO_2 surface. An electrostatic interaction takes place between positive chargers of bR and oxygen atoms located in TiO_2 surfaces, causing a transfer of a charge from bR to TiO_2. More specifically, the energy levels of bR molecules is higher than the unoccupied molecular orbital of TiO_2. When electrons get excited by light the transition of electron from bR to TiO_2 occurs without need for energy. The purpose of the redox electrolyte is to compensate for the charge that bR protein has left from electron to TiO_2. In addition, recent research has attempted to increase the amount of bR solution in order to increase the photocurrent density up to 1 mA cm^{-2}. However, putting more amounts of bR proteins creates bR multilayers, and thus impeding the photoelectrons generated from crossing the sensitizer layer and to reach the active photoelectrode. Although there are many advantages of generating photocurrent based on BSSCs, the highest efficiency is 0.35 % [26].

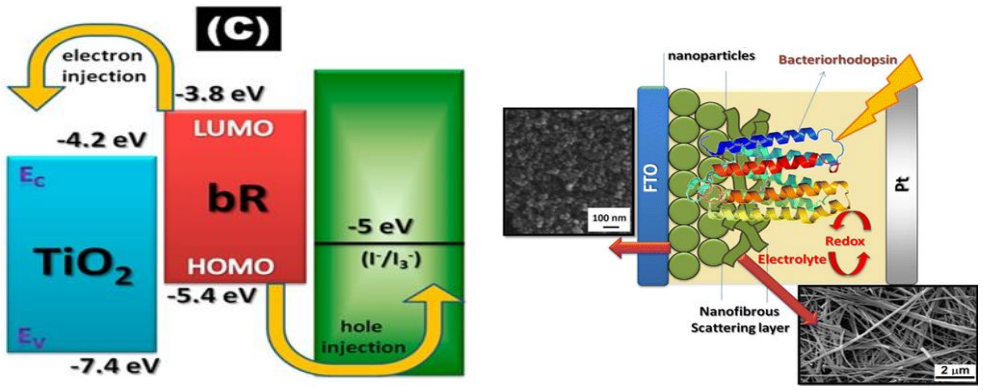

Figure 2.6 (a) BSSC energy level diagram. (b) The structure of BSSC [26].

2.3.2 Perovskite Solar Cells (PSC)

Perovskite Solar Cells (PSC) have made a revolution in this era due to its continuous progress in power conversion efficiency. Figure 2.7 (b) shows the structure of BPSC that consists

of TiO_2 layer, perovskite/mesoporous TiO_2/ bR, Spiro-OMeTAD, Au electrode and FTO glass. Figure 2.7 (a) illustrates the advantages of perovskite band (MAPbI3) where it is located below the highest occupied molecular orbitals (HOMO) of Spiro-OMeTAD and above the conduction band of TiO2. The alignments of these bands can stabilize the transfer of charge carriers. With the presence of bR molecules between perovskite and TiO_2, it helps to extend electron transfer to further points where the interference of charge recombination occurs, resulting in enhanced power conversion efficiency. It has been shown that the performance of (PSC) with bR molecules is higher; 17.02 % compared to TiO2/PSC interface 14.59%. Furthermore, it was found that the fill factor (FF) with bR molecules is responsible for improving the efficiency. That can be justified by speeding up of electron movements from perovskite to TiO_2 through bR molecules. While the absence of bR molecules causes a resistance for electron movements [27].

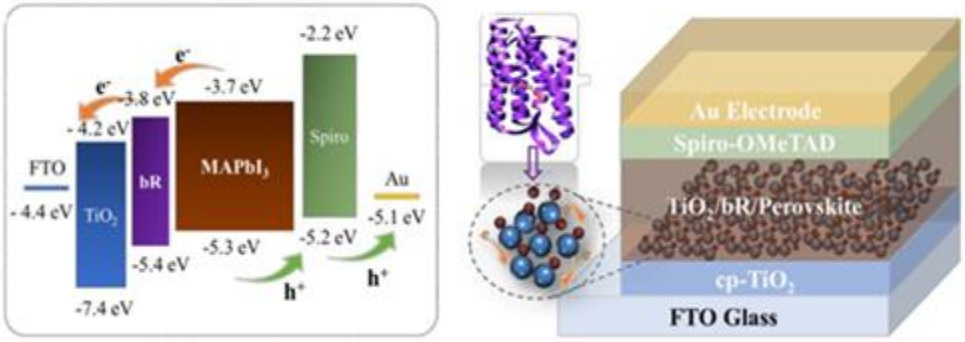

Figure 2.7 (a) Energy level diagram. (b) BPSC structure [27].

2.3.3 Hydrogen generation

Due to proton pumping of property of bR, the water splitting technique is used for photocurrent generation for bR molecules integrated into a TiO_2 nanotube. There was a big jump in efficiency performance from 2.9 to 16.5% [28]. Because of the wide range of absorption of bR/TiO_2 and the contribution of proton generation, it was shown that the maximum photocurrent

measured can reach 0.65 mA/cm^2 as compared to 0.43 mA/cm^2 for TiO_2 alone. The idea of water splitting is that electron-hole pairs (e^-/h^+) are generated when TiO_2 photoanode absorbs photons. The migration of hydrogen ions from the anode to the cathode occurs after the photogeneration. On the other hand, the photogenerated electrons move from anode to the cathode through the external circuit. bR molecules play a significant role for photocurrent enhancement producing another channel for protons. Therefore, the proton pumping property of bR protein enhances the performance. Furthermore, it was shown that absorption of a wide range of wavelengths is needed in order to get enhanced performance. Indeed, in the absence of yellow light, the photocurrent for TiO2 and bR/TiO2 is similar [29].

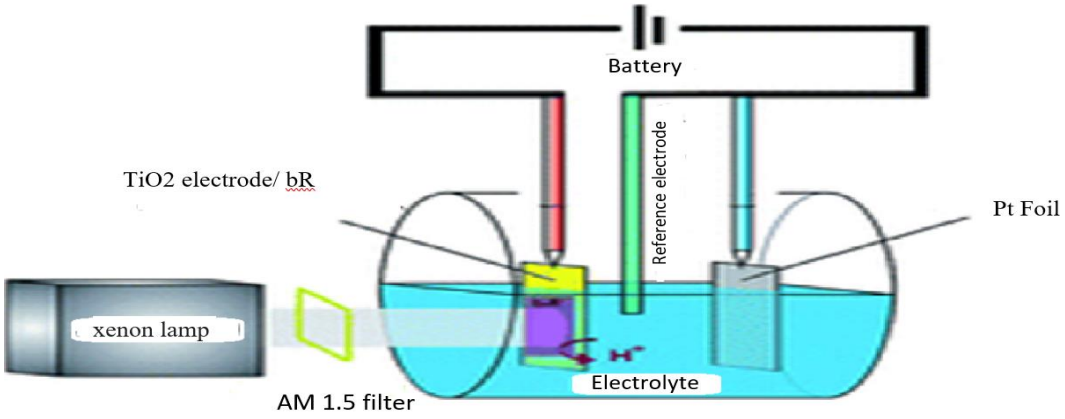

Figure 2.8 Water splitting technique [29].

2.3.4 Retinal prosthesis

bR has been currently under investigation with a high expectation that it could be offered for those who are suffering from retinal degenerative diseases. Since bR is photoactive, the bR protein can be used to treat retinal degeneration [30]. Before treating patients, a simulation of how light reacts with the bR protein can be performed using an artificial neural network to know the resolution of the system. The blindness of the retina is attributed to the death of light sensitive cells (rods & cones), which causes degenerative disease. bR proteins can activate neural

cells and therefore can been used as a replacement of these cells. An implant mimicking the absorption of homologous native visual pigments has recently been proposed [32]. The implant has a multilayered bR thin film to absorb large number of photons and is placed between ion-permeable and inert membrane surfaces. However further research is needed to increase the efficiency comparable to normal day time human vision [31].

2.3.5 Memory storage

Because of its high chemical, thermal, and radiative stability, bR has the potential to operate as a holographic recording medium in terms of reading and writing [33]. Use of bR as a volumetric memory medium has been proposed [33]. The method relies on the photocycle of bR which allows to encode binary data in terms of the bR states. Arrangement of optical elements allows one to select a small volumetric element of the bR sample can then be used for storing data (see Fig. 2.9 (a)). More specifically, application of light wavelength between 570-630 nm brings bR protein in that volumetric region from ground to an intermediate state O over a time of few milliseconds (called paging). This state O can then be excited to a state P by application of 640 nm laser, which can thermally decay to state Q. If one denotes states P or Q as bit 1 of the binary variables and 0 as the ground state of bR, one can then store data in the form of states of bR protein. The data stored can be read or erased. To read the data stored in a volumetric element, a laser light of wavelength 680 nm is shined in this region following paging. This wavelength is absorbed by two intermediate states—short-lived state K and long-lived state O. With proper timing of the laser, short-lived state K can be avoided, and the light is predominantly absorbed by state O. Hence, if the volumetric region does not absorb light it is in state P or Q (bit 1) and if the volumetric region absorbs this light, then it is bit 0. The data stored

can also be erased by shining 380nm or 490nm that bring the state P and Q to ground state. A schematic of this process is described in Fig. 2.9 (b).

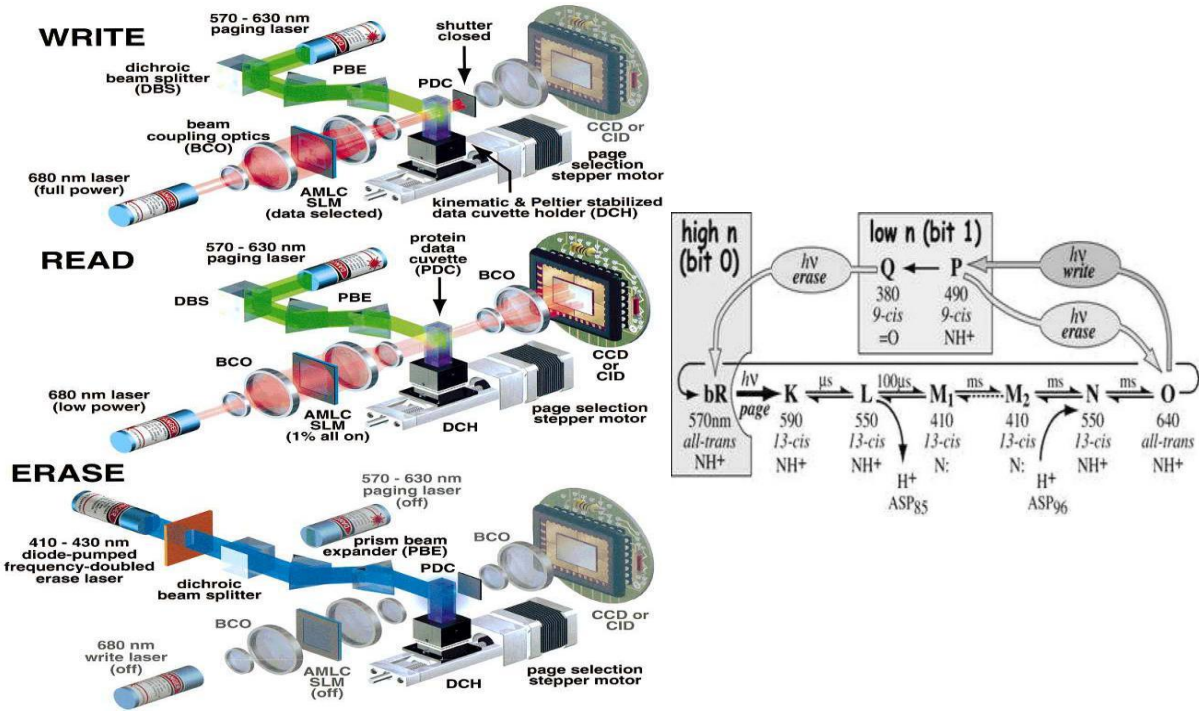

Figure 2.9 (a) The process of writing, reading, and erasing. (b) A schematic of states of bR involved in storing memory [34].

Chapter 3 : Bilayer Lipid Membranes

3.1 Definition

Cell membrane allows the cells to protect the interactions and communications that occur inside the cell from extracellular environments but also allows to interact with external environment in a regulated manner [32]. Cell membranes are made of phospholipids that can self-organize into lipid bilayers and can host proteins that can be used for interaction between inside and outside of a cell (see Fig. 3.1) [35].

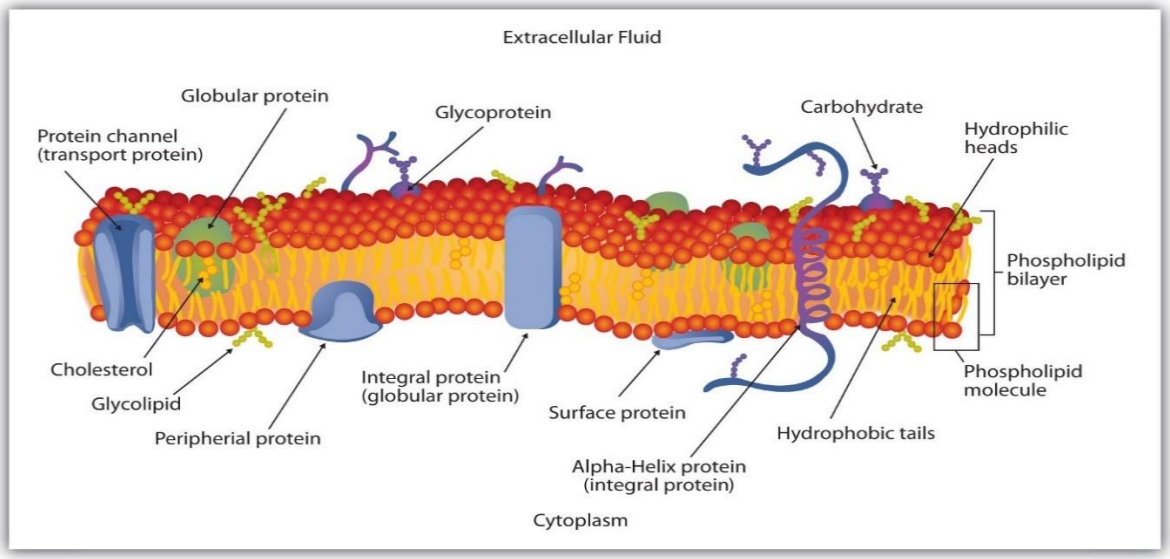

Figure 3.1 A cell lipid membrane [36]

3.2 Background

The first artificial lipid bilayer system, called black lipid membrane, was used to study the property of planar phospholipid bilayers, and is attributed to Mueller et al. [37]. The black is the dominant color of its appearance. The bilayers were formed by using lipids extracted from the brain. The system is designed with two chambers filled with conductive aqueous solution and separated by a septum. The phospholipid bilayer is formed at the septum [37]**.** Further developments let Tamm and McConnell find an approach to deposit the membrane on a solid substrate [38]. Patterns of lithographical corals from lipid bilayers was fabricated and developed by Boxer et al [39]. The Spinke and Yang have developed methods to fabricate lipid bilayers coated on various substrate such as metals, oxides, and semiconductor electrodes [40]**.**

3.3 Diphytanoyl phosphatidylcholine (DPhPC)

Due to its high stability, its low leakage of ions, and its high saturated fatty acid levels, Diphytanoylphosphatidylcholine (DPhyPC) is an ideal lipid to investigate the interaction of lipid

and the activity of the channels. Figure 3.2 shows the structure of Phospholipids is divided into two regions. The first region contains the hydrophobic fatty acid tails, and the region with letter C contains hydrophilic head group, (a) DPhPC membrane is comprised of DPhPC, (b) 3D image, (c) Kekule structure, (d) cartoon lipid molecule, and (e) lipid. The advantage of hydrocarbon chains for DPhyPC is that photo-oxidation and degradation do not have a huge influence on membrane because it has a high content of saturated hydrocarbons compared to a lipid with unsaturated ones. Additionally, the transition temperature of phospholipids is low (< 120°C) [41]**.** Using molecular dynamics simulation, a group of researchers illustrated that water diffusion through branched-chain DPhPC membrane is small compared to linear-chain DPPC [42]. This result is also verified in experiments and the resulting diminished diffusion coefficient of water is shown to arise from smaller diffusion of the hydrocarbons in the branched-chain DPhPC [41]. It was found that the water permeability of DPhPC is associated with the area of the membrane as the main factor, and the thickness of membrane comes as a secondary effect [41]**.**

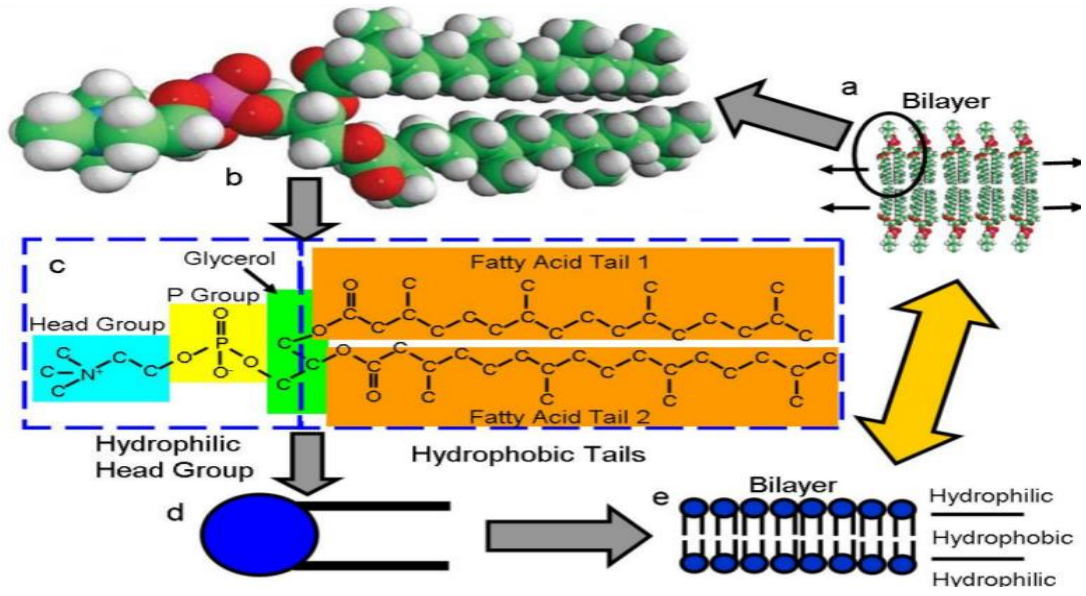

Figure 3.2 DPhyPC structure [43].

Chapter 4: Experimental setup

This chapter is devoted to the devices and approaches utilized to operate this experiment. The setup required to operate this experiment include a computer, an AC/DC converter, a patch-clamp amplifier, and a digitizer. Nevertheless, knowing the right protocol to conduct measurements were the major challenge of this work.

4.1 Faraday cage

It was important to place the formed lipid-bR membrane in a protected place to make the components function properly without causing disruptions during the photocurrent recordings. Shielding and isolating the lipid-bR solution was the approach to extract accurate results. For that reason, the experiment was implemented in a Faraday cage as shown in Figure 4.1.

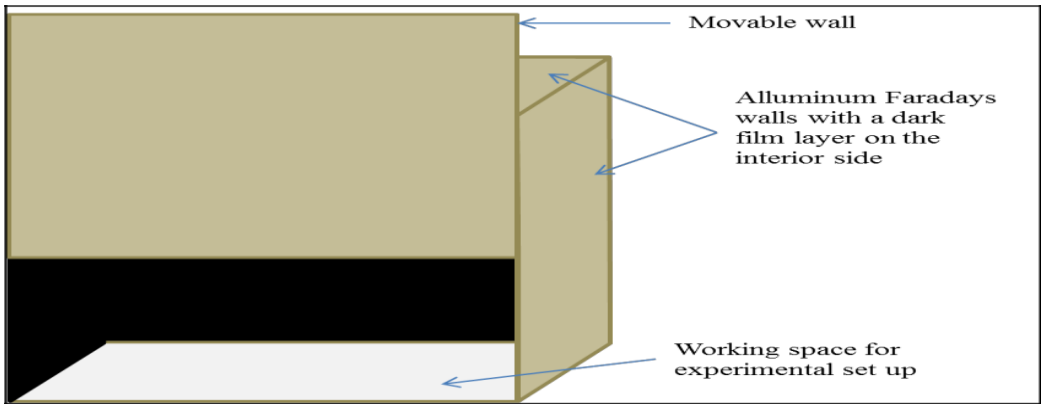

Figure 4.1 A schematic of the Faraday cage [44].

4.2 Chambers

4.2.1 Description

The two chambers were bought from Warner Instruments, USA. The system is designed with two chambers. Figure 4.2 (b) illustrates that within the large chamber, there is a second

chamber (a cup) placed inside. In addition, the cup contains a bilayer aperture of diameter 0.147mm.

Chambers are made from Polyoxymethylene (POM) that has the advantage of high solidity, low friction, and stability. The large chamber is black in color and the small one (cup) is white. Screw on the back of the large chamber plays an important role in fixing the cup with the right position for the septum (see Fig. 4.2 (a)). For example, it was necessary to avoid over-tightening the screw. To avoid overtightening, there is a rubber plug placed between the screw and the cup to prevent it from any damage. In addition, the design of the large chamber allows observers to manipulate and see what is going on inside the cell through a glass window.

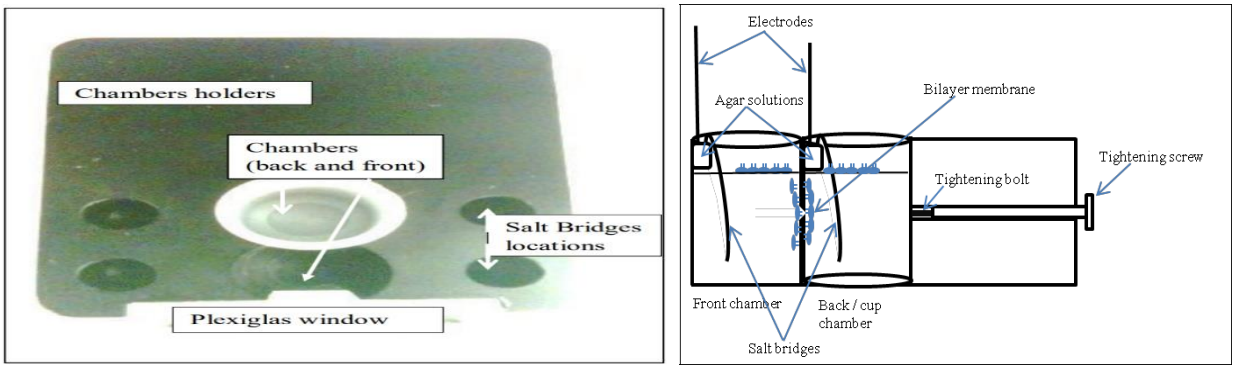

Figure 4.2 (a) The design of chambers, and (b) bilayer chamber [44]

The septum is the place where the bilayer membranes get formed across the aperture. As shown in Figure 4.2 (a). The space before the cup is identified as the front chamber, while the place where the cup is placed is known as the back chamber. In addition, there is an allocated space for the formation of salt bridges, which are responsible for maintaining charge balance in the two chambers.

4.3 Electrical Signal Measurement Setup

Electrodes, salt bridges, a digitizer, an amplifier, a head stage, the connection cables, and a computer are the components of the clamp setup. The patch-clamp technique is devoted to understanding the behavior of ion channels. In this work, the clamp system enables users to measure the capacitance and the resistance when the membrane is formed as well as the photocurrent generated.

4.3.1 Integrated Axopatch 200B Pactch Clamp Setup

Photocurrent signal is measured and recorded using an integrated Axopatch 200B patch-clamp amplifier system (Molecular Devices). It also can be used to measure the membrane's capacitance and resistance.

4.3.2 Digitizer

A digitizer Digidata 1440A (Molecular Devices, USA) was used for conversion into digital data because of its high resolution and its low noise. The digitizer is connected with an amplifier and the computer using a USB 2.0 interface. Digidata 1440A has a capacity of 16-bit data acquisition. The Digidata 1440A digitizer is connected to pCLAMP's Clampex 1 for continuous data acquisition. In addition the chambers are mounted under a microscope, AxioScope 10 (Zeiss, USA) that allows the visualization of the sample [45].

4.3.3 Headstage

A pre-amplifier (CV 203BU) was used in this work to pre-amplify the current signal, and was a part of the integrated Axopatch 200B patch-clamp amplifier system. The pre-amplifier, also known as the head-stage, plays a role in supplying the voltage through the electrodes. The head-stage is connected to the stage and the control units [46]**.** The head-stage is specifically responsible for applying voltage across the BLM and collecting the membrane potential. After

that, the amplifier receives the signal. The value of the applied voltage can be specified based on the operator's choice. The signal from the pre-amplifier was fed into an amplifier AxoPatch 200B (Axon Instruments, USA) and analyzed [47].

4.3.4 Function generator

To measure the membrane capacitance, 33250A 80 MHz was used, a waveform function generator 33250A 80 MHz was used. A 10 mV at 100 Hz triangle wave was applied for the measurement.

4.4 Salt-bridges

Agar salt bridges were used to stabilize the electrode potential. Figure 4.4 illustrates how the bridges should look and function. Salt bridges consists of 2-5% agar in 1M KCL or NaCl solution. Electrodes are immersed in the solution and the glass which is shaped as a bridge, was dipped in the agar before putting it in the electrolyte solution [48]. In general, salt bridges can only be neglected if Silver chloride electrodes are used since the photon does not react with them.

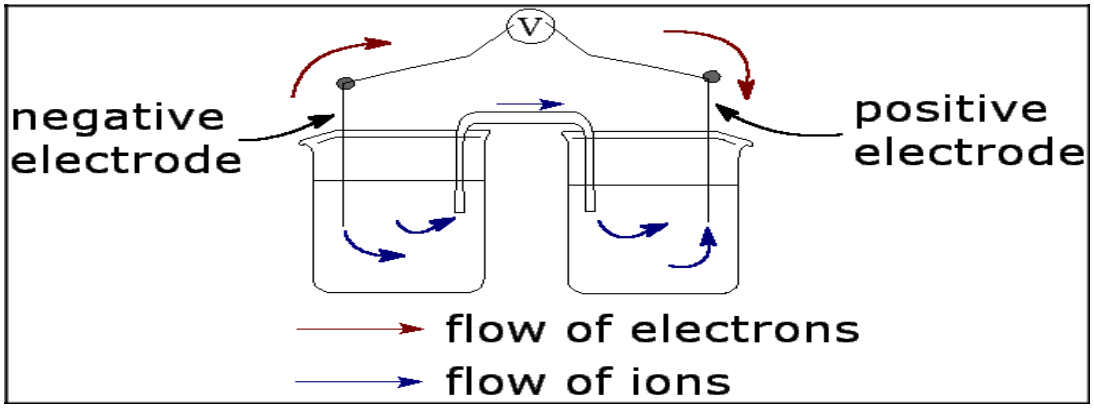

Figure 4.3 Salt-bridge principle [48].

4.5 software

4.5.1 Softwares used for data acquisition (pClamp 10)

pClamp 10 (Axon Instruments, USA) was used to acquire data. Additionally, there are many modes of data acquisition that can be obtained by using pClamp 10 [49]**.** After the acquisition of data another software, called Clampfit10, is utilized to analyze and investigate these graphs using filters. For example, it was used to find voltage spectrum and I-V curve in these experiments. In other words, Clampfit 10 enables the users to observe the data acquisition obtained from clampex.

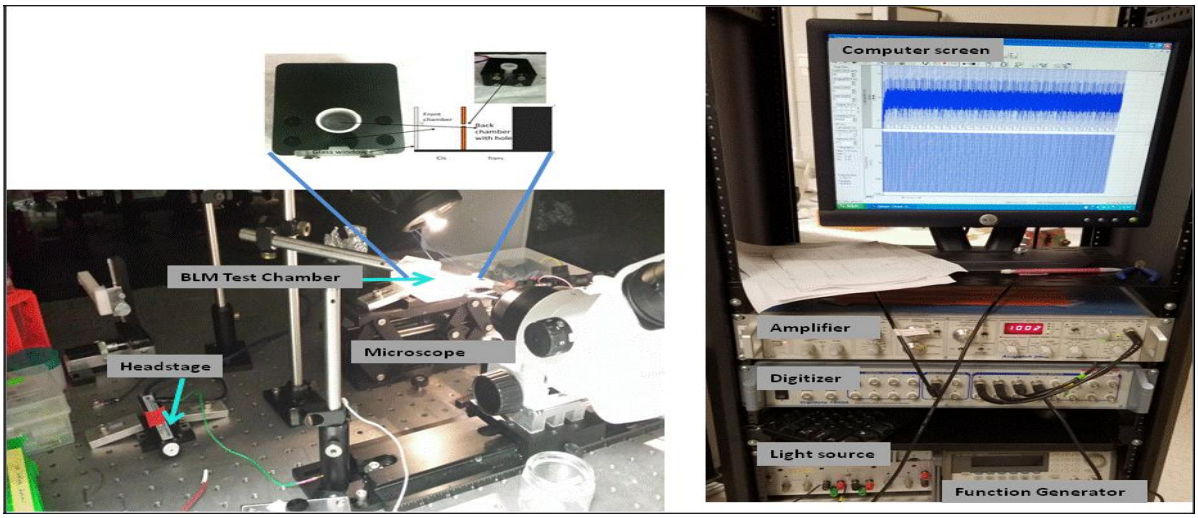

Figure 4.4 The device components [44]

4.6 Spectrophotometer

The DU800 spectrophotometer (Beckman Coulter, USAS), connected to a computer, was used to measure the absorbance of bR [50]. DU 800 spectrophotometer allows to measure the absorbance in a wide range of wavelengths (190 nm to 1100 nm).

Figure 4.5 Spectrophotometer

4.7 Power meter

The 843-R Optical Power Meter was used to calibrate the laser power. It is designed to read power from pW to thousands of watts. The power meter was obtained from Dr. Wang's lab (University of Arkansas, Physics Department).

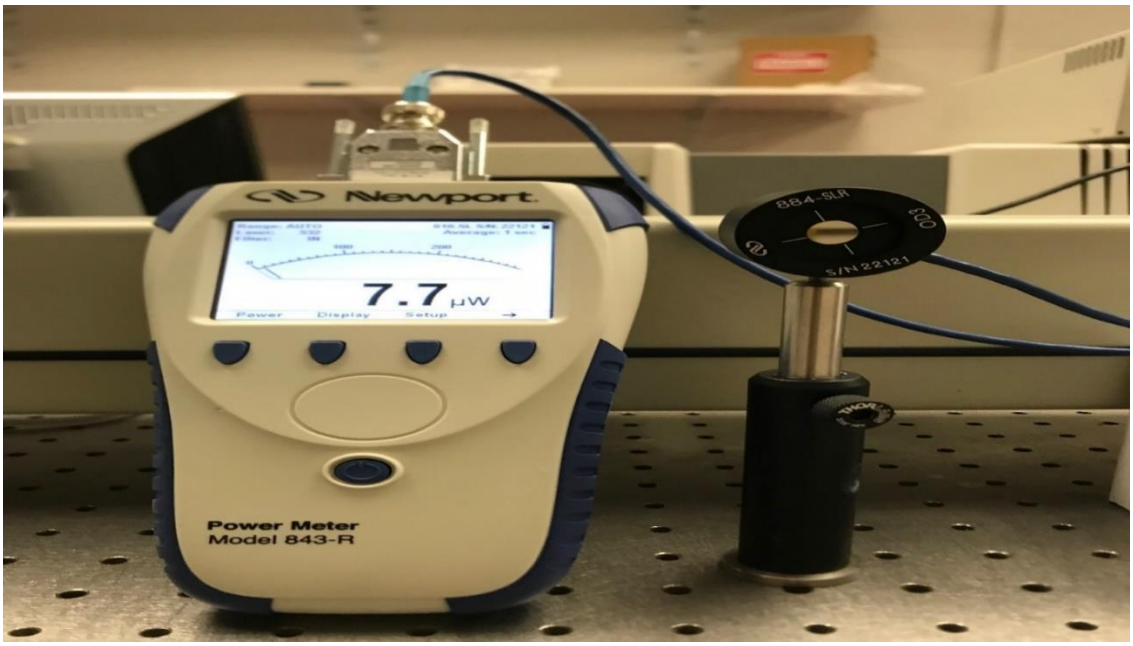

Figure 4.6 Power meter

Chapter 5: Experiment

In this section, experimental approaches starting from making biological solutions to generating a photocurrent are described.

5.1 Membrane

5.1.1 Solutions

$C_{48}H_{96}NO_8P$ (846.252 g/mol) (1,2-diphytanoyl-sn-glycero-3-phosphocholine, DPhyPC) with a purity of 99% was purchased from Avanti Lipids, USA in the form of powder [51]. Bacteriorhodopsin protein (27052g/mol) was purchased from Sigma Aldrich, USA [52]. CH3(CH2)8CH3 (n-decane) (142.28 g/mol) and KCl (74.5513g/mol) were purchased from TCI America and J. T. Baker [53][54].

Making lipid solutions is a fundamental part of this work. Therefore, DPhyPC -n-decane solution was obtained by adding 2.5 ml of n-decane to 25 mg of the DPhyPC, which represents 1

% weight per volume (w/v). After that, the lipid solution is put in small tubes and stored in the freezer at -80^{o} C. Another solution of bR and n-decane (concentration 2 µM) was made. It was required to mix the solution before placing it in the freezer. Then, the final solution was prepared by mixing 10 µl of 2 µM BR-n-decane solution and 1 µl of the DPhyPC -n-decane solution. There was no need to repeat the process of creating these solutions because these solutions can be used to perform many experiments. The final expected protein to lipid ratio was 1 bR molecule per 100-300 DPhyPC, consistent with the ratio, 1:150, of bR to lipid. 10 mM Tris-HCl, 0.1 M KCl (pH 7.4) is used as the electrolyte to fill the two chambers. The investigation of proton movement based on pH dependency has shown that the ideal range of the pH value to measure photoelectric signals should be between 4.5-8 [56]. Finally, the negative electrode (Cis) was placed in the front chamber that contained only the lipid solution (DPhyPC) with 1% w/v. While the positive electrode is placed in the back (Trans) chamber that contained bR protein and lipid solution (DPhyPC) concentration values 0.01 mg/ml and 1% w/v [55].

5.1.2 Formation of membrane

It was important that the chambers were thoroughly cleaned using HCl solution before performing the experiment. To avoid degradation of the chambers, the pH value of the cleaning solution was maintained between 4 and 9 [44]. After cleaning, the chambers were dried using argon. In addition, to simplify the adhesion of the lipid on the septum, it was important to precoat the cup-septum with lipids using a syringe by circling the syringe around the septum. It is found that the membrane formation was easier if the hole was pre-painted with the lipid solution [57].

5.1.2.1 Folding method

The development of this bilayer formation technique is attributed to Montal and Mueller [58]. Figure 5.1 shows how the folding method is used to make bilayer membrane. It can be

observed that this method tends to be more natural without human interference. Specifically, after the two compartments of chambers are filled with the electrolyte solution below the hole, the injection of the lipid solution should be placed on top of the electrolyte. That was monitored using the microscope. The last step is adding more electrolyte to both the compartments to get symmetric bilayers.

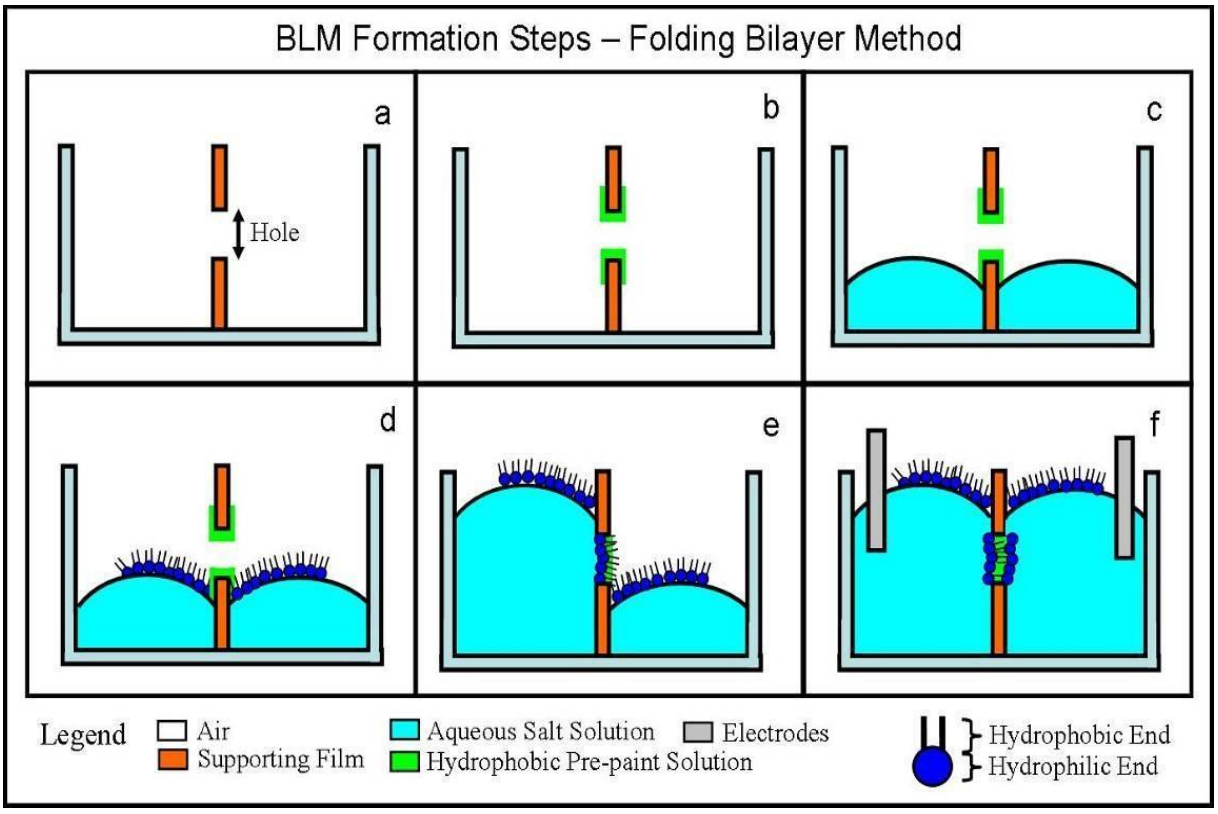

Figure 5.1 The process of folding method of bilayer membrane formation (adapted from [59]).

5.1.2.2 Painting method

The painting method is another technique used to form a membrane. In general, it is true that the folding method is more efficient in terms of forming a coherent bilayer membrane. However, the obvious disadvantage of the folding method is that it consumes larger amount of lipid or bR solution. Therefore, an alternative is the painting method of membrane formation. In

the painting method, after filling up the chamber with the electrolyte, a syringe tip containing lipid solution is dipped into the electrolyte. The membrane is formed by circling the septum hole using the syringe tip. The way of circling hole dictates if the membranes formed have multilayers or monolayers. Multilayers can be obtained by circling the hole many times by the tip, while monolayer occurs if the operator lowers number of times of circling the hole. In this experiment, bR molecules must be embedded into monolayer membrane form until the function of pumping protons can be distinguished [60].

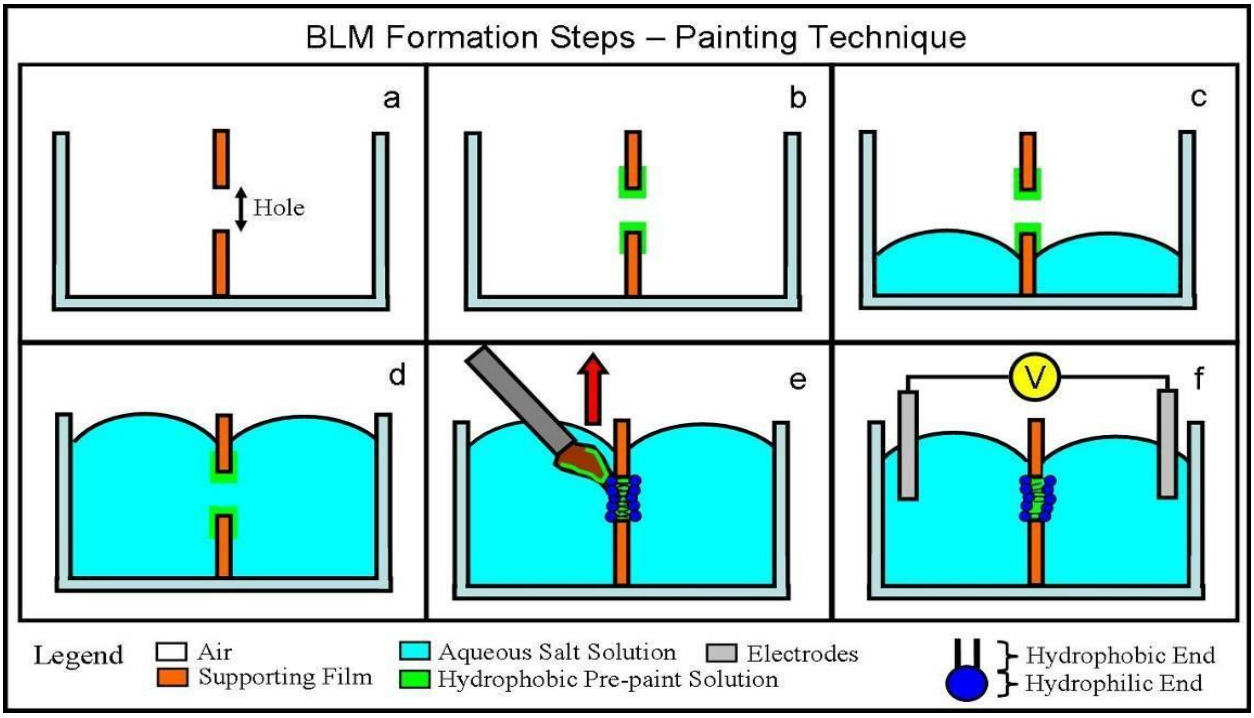

Figure 5.2 The process of painting method of membrane formation [59].

5.2 Patch Clamp Circuit

5.2.1 The electrical connections of devices

Figure 5.3 [44] explains the electrical connections among devices. In general, the generated signal goes through many phases before it gets measured. More specifically, line C1 represents the connection of the head stage with the chamber bath, while line C2 is the

connection between the function generator output and the external command rear switch. In addition, measuring membrane resistance occurs by connecting the scale output of the amplifier (line C3), where voltage signals are generated, with channel 0 located in the digitizer. However, channel 3 of the digitizer was connected to the generator output by a “T-joint”. The response of signals was observed on the computer screen by connecting the 10 mV output of the amplifier with channel 1 of the digitizer (line 4). Also, the generated current was observed on the computer screen by connecting the 10 kHz output of the amplifier with channel 2 of the digitizer (line 5). Line 6 illustrates the connection of the digitizer analog output and the second external command of the amplifier. In this connection, the voltage signal produced to investigate and evaluate the membrane resistance was transmitted by the cell. Finally, it was necessary to make a group of connections between the Gain, Frequency, and Cell capacitance (“telegraph outputs”) of the amplifier with channels 0, 1 and, 3 of the digitizer telegraph input (line7, line 8, line 9) to observe the properties of the membrane. It was necessary to use the Clampex program to investigate the connections among these devices [44].

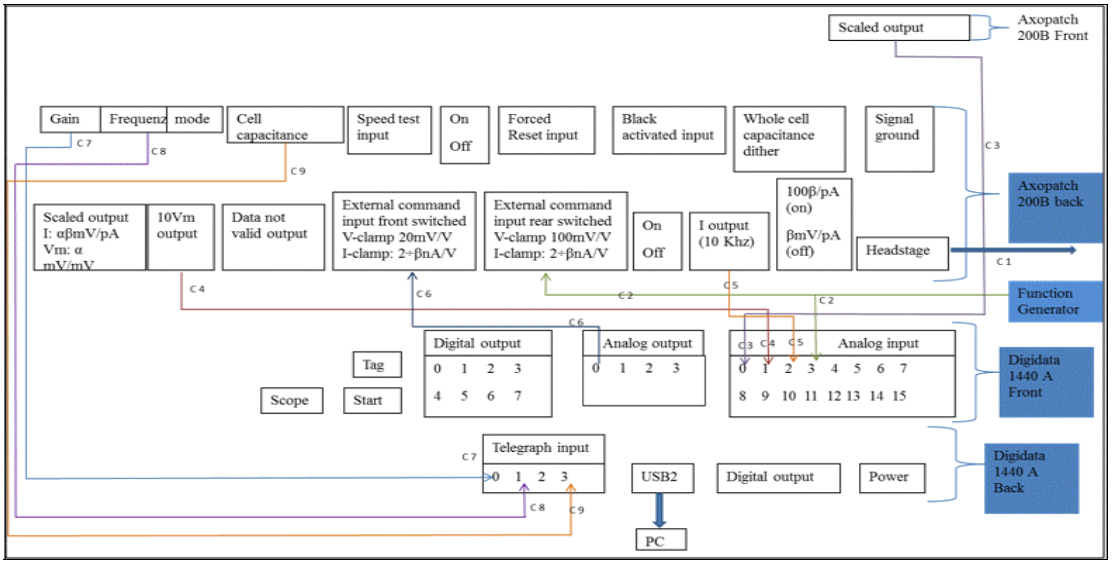

Figure 5.3 The electrical connection of devices [44].

5.3 The dynamicity of membrane capacitance under electric field

Figure 5.4(a) and (b) explain the behavior of the membrane with and without electric field. More Specifically, applying electric field across the membrane is accompanied by emerging phenomena called electrocompression. It causes reduction in membrane thickness due to attractive coulomb forces. It has implications for the measurements of membrane capacitance. However, as the AC voltage is reduced, the membrane thickness returns to its initial states due to the combination of applied electric field and the repulsion between layers [61].

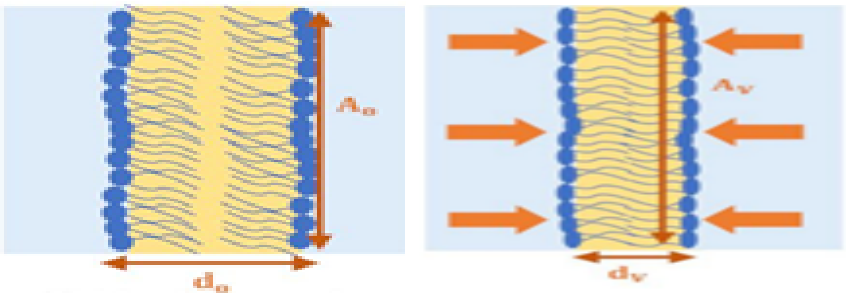

Figure 5.4 Thickness of membrane (a) without an electric field, and (b) with application of electric filed [61].

5.4 The dynamics of membrane resistance

As illustrate in Figure 5.5 (a) and (b) [61], the main goal of performing conductance measurements by applying DC voltage is to testify the permeability of lipid membrane. Unmodified lipid membranes are not permeable to ions. However, it has been shown that some modified planar lipid bi-layer membranes can conduct transmembrane ionic transport without peptides or proteins [64]. Specifically, transmembrane potential arises due to a combination of membrane surface potential and dipolar potential [61]. Figure 5.5 (b) illustrates this phenomenon. In the absence of any channel-forming proteins, the dipole and surface potential of the interfaces are similar and thus the membrane has a very high resistance (typically of the order of giga-Ohms). In the presence of channel-forming proteins, such as bR in this case, the

resistance of the membrane decreases. Application of DC voltage increases the current across the membrane. However, application of very large voltage across the membrane may lead loss of binding of peptides to membrane [63].

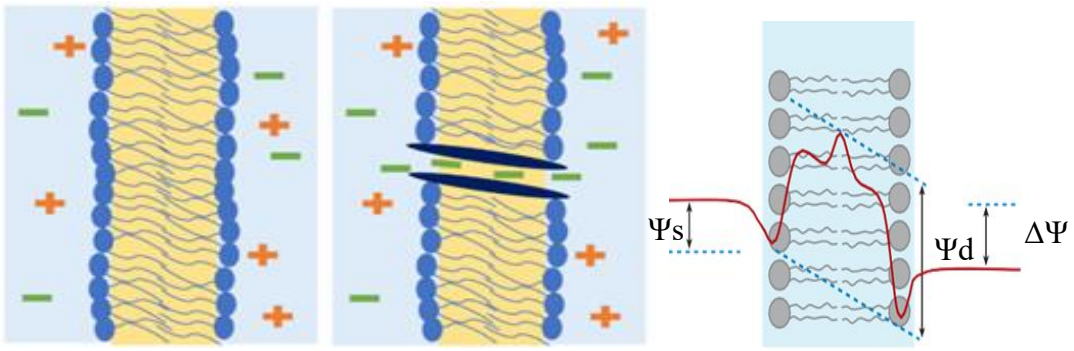

Figure 5.5 Application of DC voltage on membrane in the presence and absence of channel-forming proteins [61]. (b) Selective ion transport leads to an imbalance of membrane potential [62]

5.5 Measuring Membrane Capacitance

Membrane capacitance arises due the dielectric permeability differences between the surface and the inner hydrophobic part of the bilayer. The hydrophilic part of the lipid-bilayer is in contact with the solvent (primarily water with dielectric constant ~80), while the inner hydrophobic core of the bilayer has a very small dielectric constant (~2) [58,62]. Therefore, a bilayer could be considered as a capacitor in parallel with a resistance.

The protocol chosen to do this work was voltage clamp ramp protocol (VC- ramp). A voltage of 10 mV amplitude (peak to peak with -5 mV to +5 mV) at 100 Hz was applied using the function generator and the current was measured as shown in Figure 5.7 [44]. Nevertheless, it was important to divide the value of current by 2 due to the symmetric voltage during the ups and downs of ramps. Also, it was taken into considerations that the ramps of voltage were selected from the middle of output current and the applied voltage to obtain accurate measurements for the membrane capacitance [65].

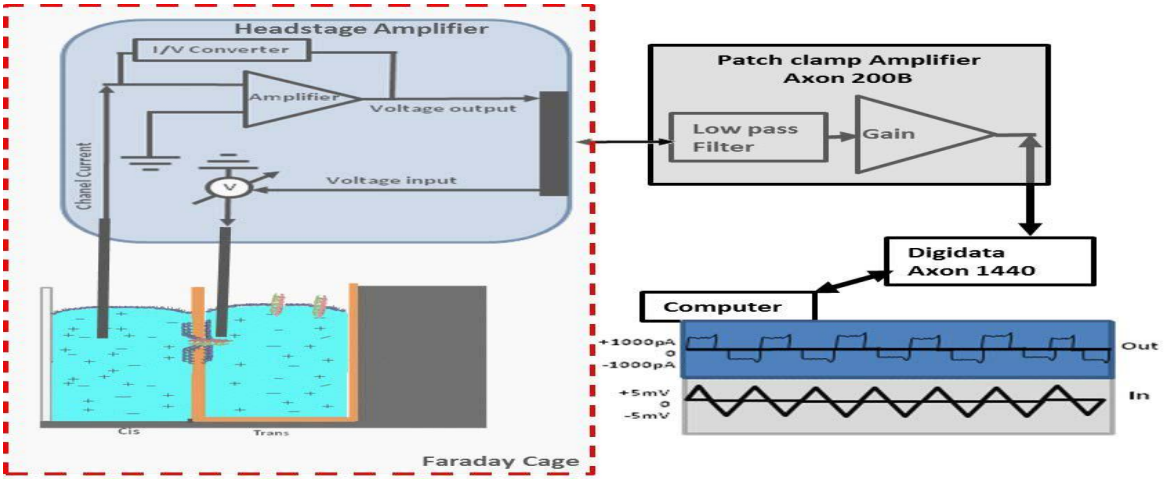

Figure 5.6 The image of system with voltage ramps and output current [44].

The capacitance was calculated using Equation 5.1 where, ΔQ is the charge, ΔV is the applied voltage, I is the current, and Δt is the time duration.

$$C = \frac{\Delta Q}{\Delta V} = I \times \frac{\Delta t}{\Delta V} = \frac{\varepsilon_0 \, \varepsilon_r \, A}{d} \qquad \text{(Equation 5.1)}$$

In addition, the value of capacitance was obtained by identifying A, the area of membranes (cm^2), d the thickness of membranes or the distance between two membranes (nm), (ε_0) the dielectric constant of the vacuum (equal 1), and ε_r the dielectric constant of the material (F/cm).

5.6 Measuring Membrane Resistance

Membrane resistance was measured by applying a steady DC voltage using the amplifier where the leakage of current can be measured. In order to get the I-V curve without causing huge changes in the membrane structure, +/-100 mV range was chosen from clampfit protocol. The inverse of the resistance was calculated from the slope of the I-V curve.

$$R = \frac{V}{I} \qquad \text{(Equation 5.2)}$$

Ohm's-law is defined as R, the resistance in gigaohm (GΩ), V, the voltage in millivolts (mV) and, I, the current in picoampere (pA).

5.7 Photocurrent

In order to observe the unique proton pumping property for bR protein, it was necessary to focus the laser beam on the membrane. Otherwise, the photocurrent generation due to translocating protons between the chambers would not occur while turning the laser off and on. It was observed that there were two opposite transient spikes in current accompanied by turning the laser on and off. The spike generated due to turning the laser on is because of release of protons bR undergoes transition from the ground state to M state. With the continuation of turning the laser on, the proton builds up in the M state resulting in a temporary block followed by uptake of protons when the laser is turned off. For this reason, there is a sudden drop [66]**.**

Chapter 6 : Results and Discussion

6.1 Results

The painting method and the folding method were the two approaches used to perform these experiments. It was expected that the results obtained using the painting method are less accurate compared to the results obtained using the folding method. That can be justified by the fact that the operator's intervention was required to form the membrane for using the painting method. In other words, the accuracy of results using this method is related to the operator's confidence and qualification. For that reason, the folding method was chosen to generate photocurrent which also helps avoiding creating bubbles in which may interfere with laser focusing.

6.2 Laser calibration

To guarantee the success of this work, calibrating the laser was an important step. More specifically, the first step to was if the laser (green 532 nm) is capable of pumping protons or not when it strikes bR-membrane system. I first calibrated the power incident on the membrane system by moving the laser away from it at different positions and measuring the laser power. As the distance of the laser form the membrane sample increases, the power gradually decreases as shown in Fig. 6.1. The distance was varied between 23 cm and 150 cm. The laser power at 23 cm was measured to be 91 mW, after that, there was a continuous decrease in power with distance. At the distance of 150 cm, the lowest value recorded for the laser power was 81 Mw. In this work, distance between the laser and the membrane was fixed at 23 cm (yellow dotted line in Fig. 6.1). However, the intensity of laser is not the only criteria for the bR protein to pump protons. The concentration of hydrogen ions play a significant role in pumping protons. For example, it was observed that the action of proton pumping depends on the concentration of hydrogen ions. Whenever pH value of the solution increases, the light intensity should be higher to pump protons. Moreover, pH value depends non-linearly on laser intensity due to depletion of protons arising due to pumping [67].

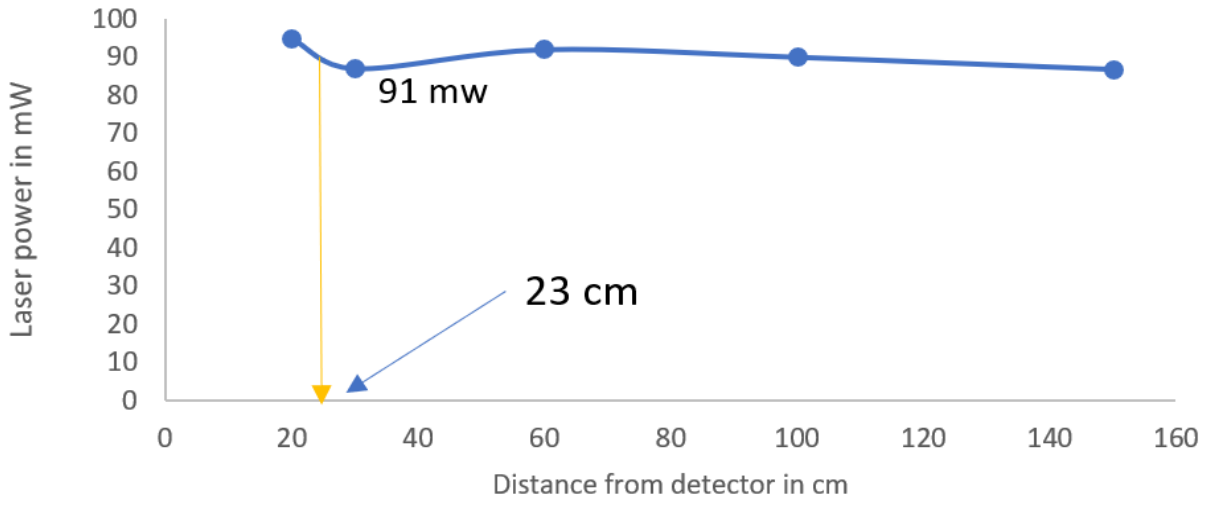

Figure 6.1 Calibration of intensity of green laser (532 nm).

6.3 Absorption spectrum

The analysis of the absorption properties of Bacteriorhodopsin was performed to identify the range of absorption wavelengths of bR. UV -VIS spectroscopy is the most common approach widely used among scientists. The idea of UV-VIS spectroscopy is to detect the intensity of radiation of different wavelengths passing through the protein solution. Larger absorption corresponds to lower intensity detected.

The experiment was prepared by mixing 20 µl of the protein solution with 180 µl of a 0.1 M KCl in a tube before putting it in a cuvette. After that, another cuvette filled with 200 µl of the 0.1 M KCl solutions was used as a reference. The absorption spectrum was obtained for the wavelength range between 300 nm to 900 nm. The protein absorption spectrum obtained is shown in Figure 6.2. Absorption peak for the protein is observed around 563 nm. Also, it was seen that there was a small dip (0,6057 counts) at 575.5 nm that may arise due to impurities in the solution inside the cuvette. Figure 6.2 suggests that the wavelength range associated with the activity of Bacteriorhodopsin is between 457.5 nm to 652.5, consistent with the literature.

By identifying the maximum absorbance peak of the spectrum, the molar concentration was calculated using the Beer- Lambert law (Eq. 6.1).

$$A = \varepsilon \, l \, c \qquad \text{(Equation 6.1)}$$

where A is the maximum absorbance, ε is the molar absorption coefficient (M^{-1} cm^{-1}), *l* is the optical path length (cm), and c is molar concentration (M). By using the value of the absorbance, A (0,6359), ε (63000 M^{-1} cm^{-1}), and *l* the optical path length (1 cm), we obtained a value of 10.09 µM for the concentration of the protein.

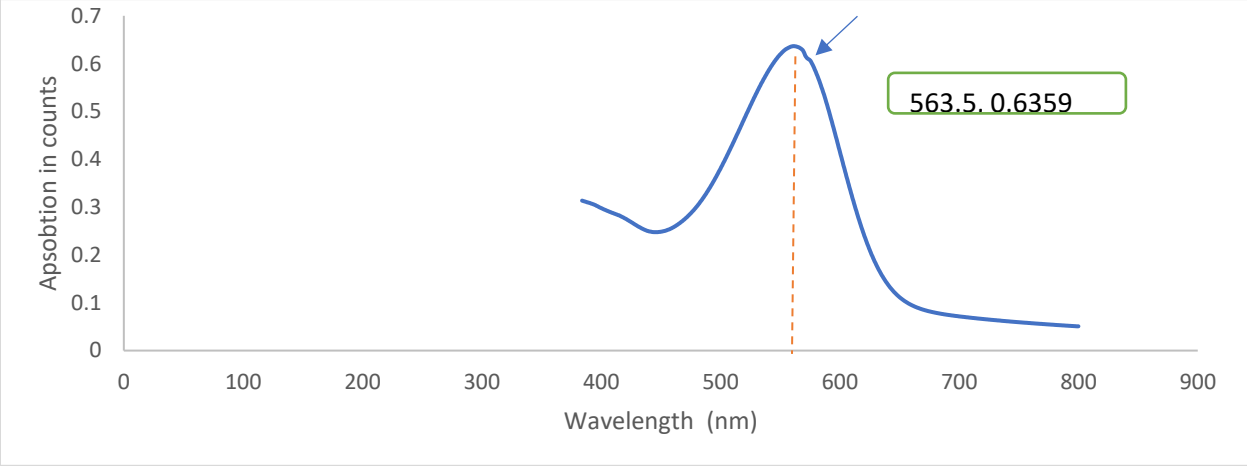

Figure 6.2 Absorption spectrum of bR.

6.4 Membrane resistance

6.4.1 Membrane formed with painting method

The I- V curve was obtained as illustrated in Figure 6.3 after applying a DC voltage between - 100 mV and +100 mV across the membrane. The output current was plotted against the voltage and the resistance was obtained from the inverse of the I-V curve by fitting a straight line through the curve.

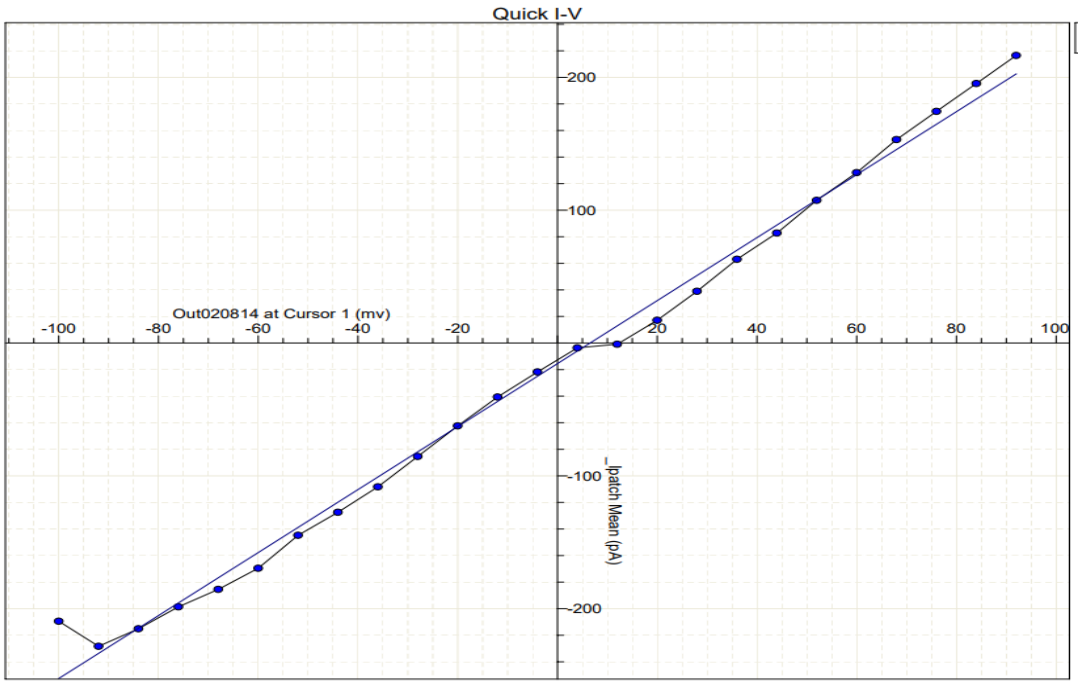

Figure 6.3 I-V curve for membrane obtained using the painting method.

The typical value of membrane resistance should be equal or greater than 0.1 GΩ [68]. The value of the membrane resistance obtained in my experiment was 0.42 GΩ

6.4.2 Membrane formed using folding method

In this part, the membrane was obtained using the folding method and the experimental I-V curve is shown in Figure 6.4. The calculated value of the resistance was 0.38 GΩ, which is close to the reference data [68].

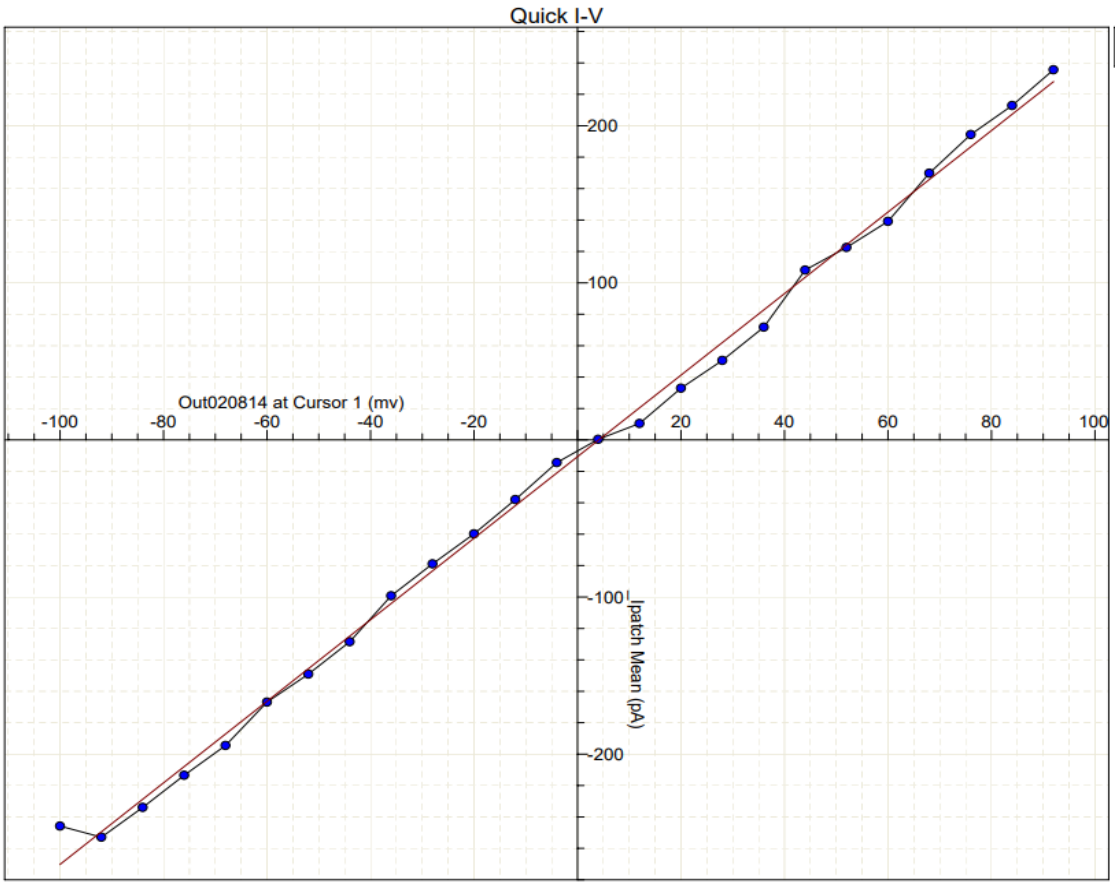

Figure 6.4 I-V curve for membrane obtained using the folding method.

The I-V curve was smoother for the membrane formed using the folding method as compared to the membrane formed using the painting method. More specifically, the symmetrical membranes are the major reason for better I-V curve for the membrane using the folding method.

6.4.3 Membrane containing bR proteins using folding method

Since folding method gives a better result for the membrane, we performed the resistance measurement of bR-membrane system (without laser) using the folding method. The previous Figures explained how the I -V curves look like in the presence of the DPhyPC + n-Decane only. Figure 6.5 shows the I-V curve for the bR-membrane (bR- DPhyPC + n-Decane) system

obtained using the folding method. The value the resistance obtained in this case is 0.48 GΩ. It is noticeable that the resistance has a slightly higher value than that of in bR- Free membrane. This may arise due to membrane stability increase due to the incorporation of bR proteins into the membrane. In other words, the attenuation of current has been attributed to the binding of a guest bR molecule.

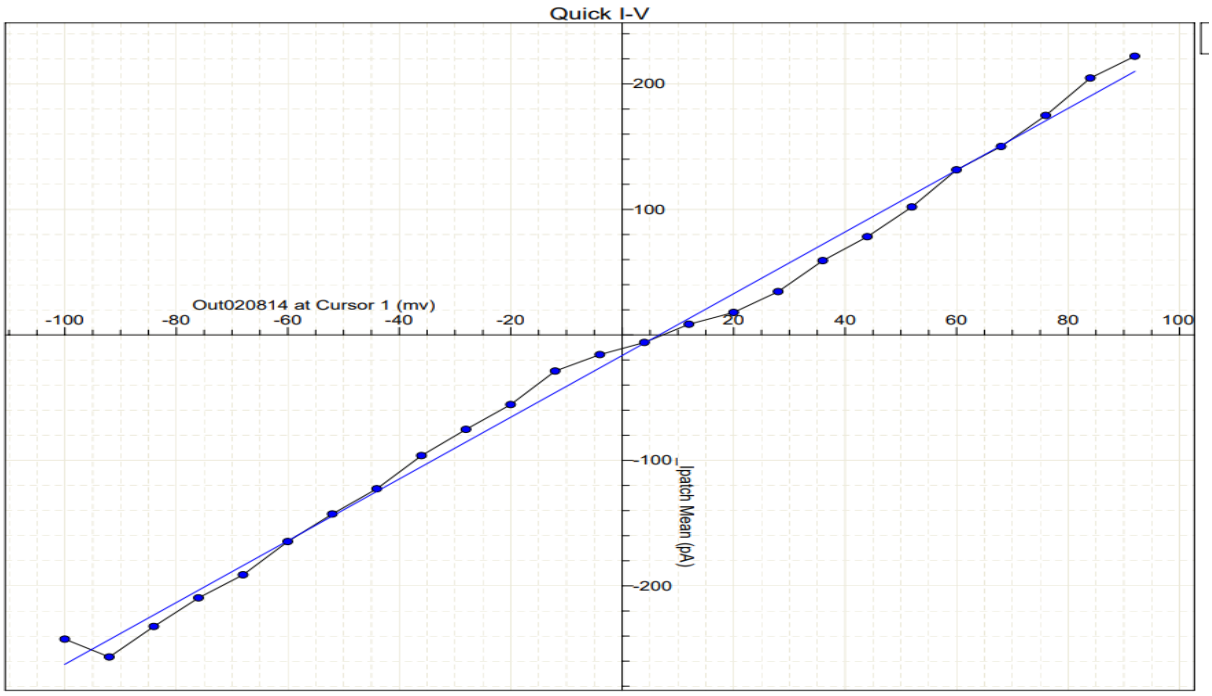

Figure 6.5 I-V curve for bR-membrane system obtained using the folding method.

6.5 Membrane capacitance

Membrane capacitance was measured by applying a triangular voltage waveform across the membrane using the function generator and the current was recorded. The capacitance was calculated from the time dependence of the voltage and the current (see Fig. 6.6). The values of the capacitance depended on the method used for membrane formation. We find that the value of the capacitance was smaller (0.172 uF/cm^2) for the membrane formed using the painting the method as compared to capacitance (0.205 uF/cm^2) for the membrane formed using the folding

method. Usually, membrane formed using the painting method leads to monolayer membranes, for that reason, the capacitance has a lower value compared to the folding method that results in bi-layer membranes. In addition, the value of membrane capacitance goes up (0.75 uF/cm^2) when bR molecules are inserted into the lipid membrane. This increase in the capacitance is attributed to the capacity of storing more opposite charges on the membrane.

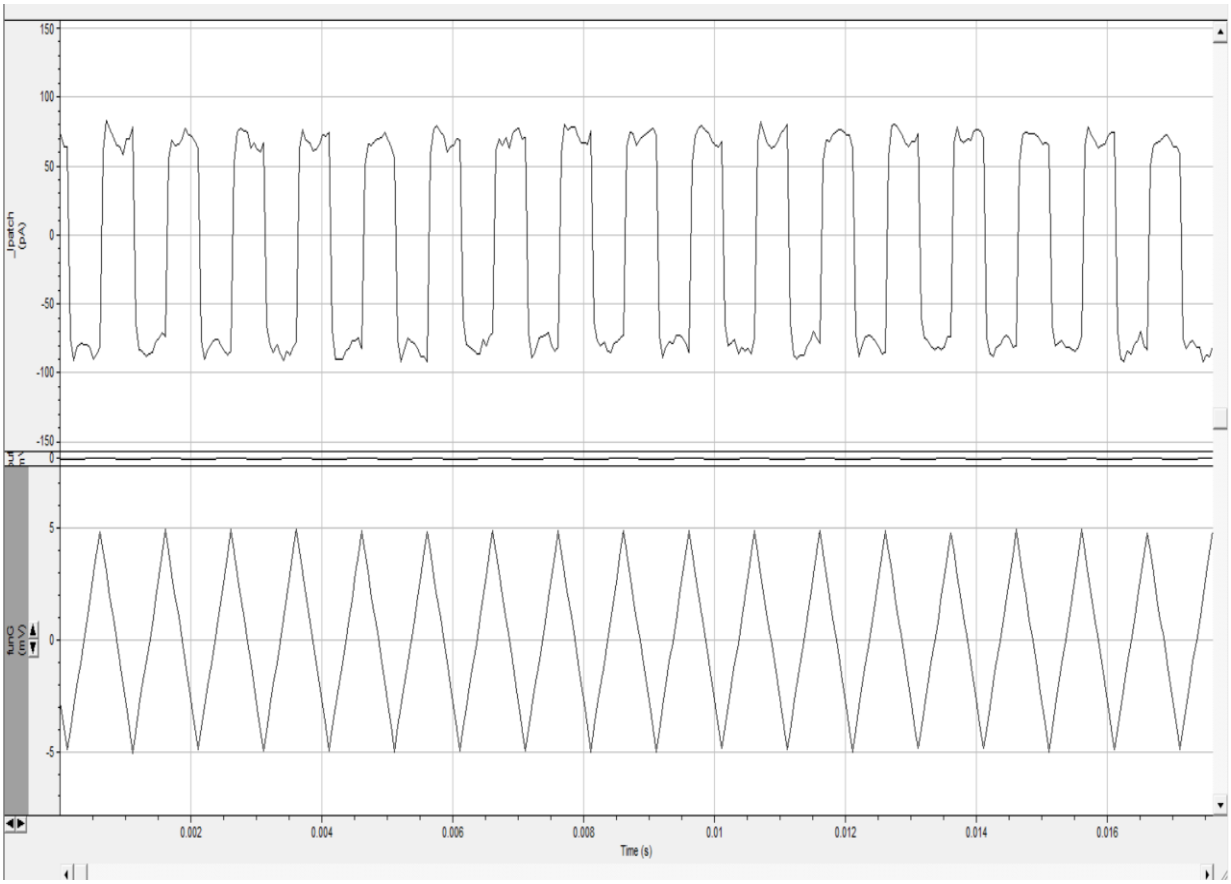

Figure 6.6 Capacitance measurements from the time dependence of the current and voltage.

6.6 Shinning laser on bR free membrane

Figure 6.7 explains the effect of laser on the bR- free membrane. It was first important to test how the photocurrent signal behaves when the laser hit the membrane comprised of the DPhyPC+n- Decane solution only (without bR). Folding method was used to form the

membrane. Since the membrane is free of bR proteins, there is no net current observed even in the presence of laser.

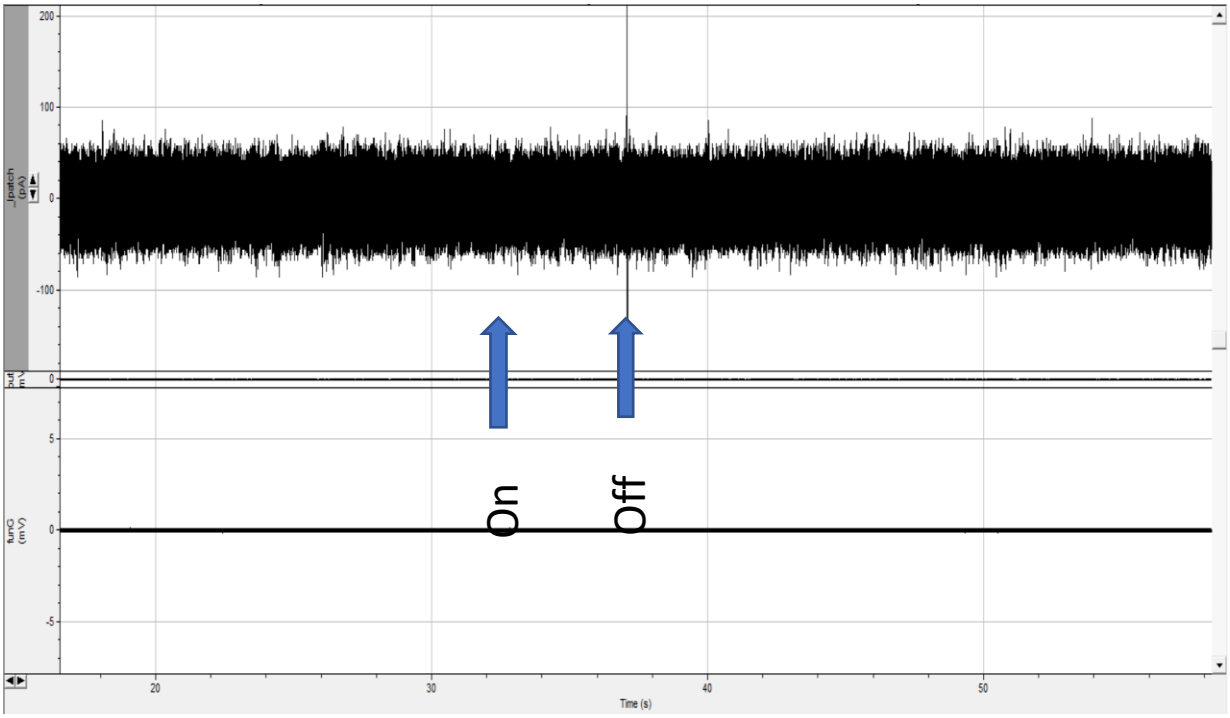

Figure 6.7 Photocurrent when irradiating the membrane with the laser on bR-free membrane.

6.7 Generating photocurrent signals using the folding method

Figure 6.8 shows the three transient spikes of photocurrent produced under no voltage applied when the bR-protein system is irradiated with the laser. When the laser is turned on, the protons translocated from one compartment to another, leading to an increase in current. This happens over a time of 100ms after the laser is turned on, followed by a drop due to the reduction of protons diffusion after the laser is turned off. On the other hand, looking closely at the signals of generated photocurrent, the generation of photocurrent for the first two signals is a little bit larger than the third one when the membrane is irradiated for a longer time. On keeping the light on for a longer period, protons are depleted due to pumping. In the other words, there may not be protons available to pump. For that reason, the third signal of photocurrent produced has a lower value. As shown in Figure 6.8, the value of photocurrent density generated is (5.3-7.1pA/cm^2)

which is still far from (300 nA/cm^2) achieved in Ref. [68]. It is noticeable that the signals cannot go back to zero immediately until the proton uptake occurs with negative signals, then it goes back to the initial level.

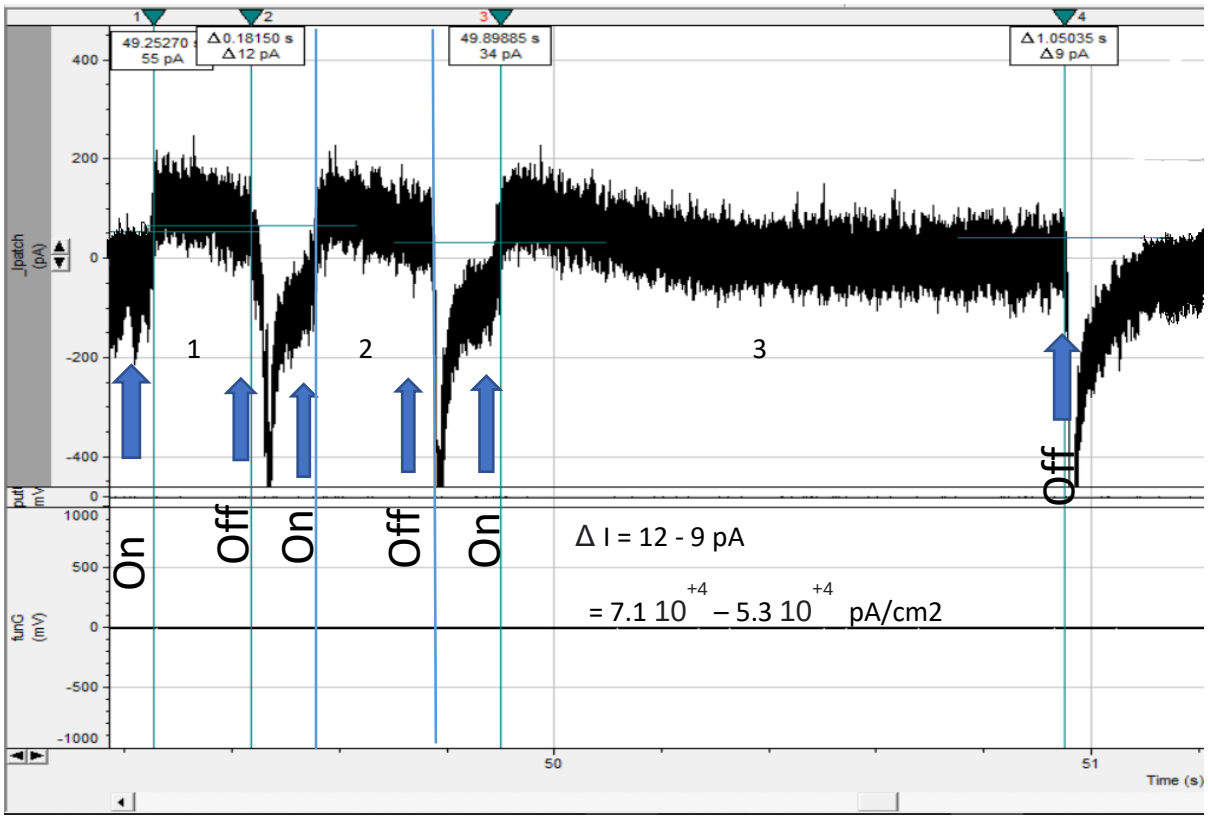

Figure 6.8 Generation of photocurrent upon irradiating the bR-membrane system with laser. The bR-membrane system was formed using the folding method

6.8 Discussion

In this work, the uniqueness of proton pumping ability of bR protein was successfully observed. Many factors should be taken into consideration. One of them which represents a big challenge for a lot of scientists is about dealing with the ratio between bR and DPhyPC. Although 0.1 M KCl was the appropriate concentration to operate the experiment, it was recommended to prepare the buffer solution with 1 M KCl or 1M NaCl [69].

It is still desirable to orient protons in bi-layer membranes to generate more photocurrent signals since there is no way to reduce the photocycle of bR. Also, studying the impact of the electrolyte pH on the proton flux is necessary to understand the ideal contact between solution (for example , K^+) and membrane.

Figure 6.7 and figure 6.8 show how the response of lipid membrane formed on light with and without bR molecules using the same buffer in both sides of the membrane. That confirms that observing photocurrent is only linked with the presence of bR molecules. The photocurrent observed was evidence of the compatibility between bR protein and lipid membrane. Also, the two transient spikes observed are fit with the function of the bR photo-cycle. To clarify, regulating the pumping of protons started from watching transient peak due to induced charge upon illumination. The gradual decrease of transient peak represents the diffusion of protons ending with refilling up the Schiff base when the laser is off.

Summary and conclusion

Hosting bR molecules requires to build a good foundation for the capacity and the resistance to hold these molecules. For that reason, measuring the membrane capacitance and resistance for lipid membrane was the key to evaluate this task. Painting and Folding were the methods evaluated to choose the most efficient one to host bR molecules. It was found that the folding method is more efficient due to forming bi-layer membranes.

The results extracted from this work confirmed that these setups followed to generate photocurrent is a good standard for future work of lipid-protein membrane bases. Also, it is highly recommended to play with the experimental parameters to increase the pumping of protons. One of these parameters is to increase the concentration of the bR protein. Also, the influence of voltage dependency on the bR photocurrent generated.

Although there are many advantages of using black lipid membrane to form phospholipid bi-layers, observing the interactions on the membrane surface represents an obstacle. Therefore, using solid supports to deposit phospholipid bilayers is another method emerged to do that task. One of these powerful tools is using atomic force microscopy to analyze what is going on the membrane surface. However, the negative aspect of method is that there is a possibility of preventing transmembrane proteins (immobile) to interact with the underlying substrate since the supported membrane is not completely separated from the underlying substrate [35].

References

1. ogers, K. (2018, February 6). Rhodopsin. Encyclopedia Britannica. https://www.britannica.com/science/rhodopsin

2. Stoeckenius, W. (2008). Bacterial rhodopsins: Evolution of a mechanistic model for the ion pumps. *Protein Science, 8*(2), 447-459. doi:10.1110/ps.8.2.447.

3. Bank, R. (2021). RCSB PDB - 1FBB: CRYSTAL STRUCTURE OF NATIVE CONFORMATION OFBACTERIORHODOPSIN. Retrieved 4 November 2021, from https://www.rcsb.org/structure/1fbb

4. Henderson, R. (1977). The purple membrane from halobacterium halobium. *Annual Review of Biophysics and Bioengineering, 6*(1), 87-109.

5. Biology Libretexts. https://bio.libretexts.org/Bookshelves/Micro

6. RICHARD H. LOZIER, & ROBERTO A BOGOMOLNI.*Bacteriorhodopsin: A light-driven proton pump in halobacterium halobium.*

7. Renugopalakrishnan, V., Barbiellini, B., King, C., Molinari, M., Mochalov, K., & Sukhanova, et al. (2014). Engineering a Robust Photovoltaic Device with Quantum Dots and Bacteriorhodopsin. *The Journal Of Physical Chemistry C, 118*(30), 16710-16717. doi:10.1021/jp502885s.

8. Yao, B., Xu, D., Hou, X., Hu, K., & Wang, A. (2001). Analyses and proofs of multiexponential process of bacteriorhodopsin photoelectric response. *Journal Of Applied Physics, 89*(1), 795-797. doi: 10.1063/1.1329661.

9. Jin, Y., Honig, T., Ron, I., Friedman, N., Sheves, M., &Cahen, D. (2008). Bacteriorhodopsin as an electronic conduction medium for biomolecular electronics. *Chemical Society Reviews, 37*(11), 2422-2432.

10. H. Michel and D. Oesterhelt. 1976. “Light-induced changes of the pH gradient and the membrane potential in Halobacterium halobium”. FEBS Lett. 65, pp. 175–178.

11. Nagel, G., Kelety, B., Möckel, B., Büldt, G., & Bamberg, E. (1998). Voltage Dependence of Proton Pumping by Bacteriorhodopsin Is Regulated by the Voltage-Sensitive Ratio of M1to M2. *Biophysical Journal, 74*(1), 403-412. doi: 10.1016/s0006-3495(98)77797-5.

12. Henderson, R., & Unwin, P. (1975). Three-dimensional model of purple membrane obtained by electron microscopy. *Nature, 257*(5521), 28-32. doi: 10.1038/257028a0

13. Hasegawa, N., Jonotsuka, H., Miki, K., & Takeda, K. (2018). X-ray structure analysis of bacteriorhodopsin at 1.3 Å resolution. *Scientific Reports, 8*(1), 13123-8. doi:10.1038/s41598-018-31370-0.

14. Kandori, H. (2000). Role of internal water molecules in bacteriorhodopsin. *Biochimica et BiophysicaActa (BBA)-Bioenergetics*, *1460*(1), 177-191.

15. Hirai, T., & Subramaniam, S. (2003). Structural insights into the mechanism of proton pumping by bacteriorhodopsin. *FEBS letters*, *545*(1), 2-8

16. Lanyi, J. K. (2004). X-ray diffraction of bacteriorhodopsin photocycle intermediates (review). *Molecular Membrane Biology*, *21*(3), 143-15doi:10.1080/09687680410001666345

17. Der, A., &Keszthelyi, L. (2001). Charge motion during the photocycle of bacteriorhodopsin. *Biochemistry (Moscow)*, *66*(11), 1234-1248. doi:10.1023/A:1013179101782

18. Wang, T., Facciotti, M., & Duan, Y. (2013). Schiff Base Switch II Precedes the Retinal Thermal Isomerization in the Photocycle of Bacteriorhodopsin. *Plos ONE*, *8*(7), e69882. doi:10.1371/journal.pone.0069882

19. Nango, E., Royant, A., Kubo, M., Nakane, T., Wickstrand, C., Kimura, T., ... & Iwata, S. (2016). A three-dimensional movie of structural changes in bacteriorhodopsin. *Science*, *354*(6319), 1552-1557.

20. Onufriev, A., Smondyrev, A., & Bashford, D. (2003). Proton affinity changes driving unidirectional proton transport in the bacteriorhodopsin photocycle. *Journal of Molecular Biology*, *332*(5), 1183-1193.

21. Zimanyi, L., Varo, G., Chang, M., Ni, B., Needleman, R., & Lanyi, J. K. (1992). Pathways of proton release in the bacteriorhodopsin photocycle. *Biochemistry*, *31*(36), 8535-8543.

22. Nogly, P., Weinert, T., James, D., Carbajo, S., Ozerov, D., Furrer, A., . . . Standfuss, J. (2018). Retinal isomerization in bacteriorhodopsin captured by a femtosecond x-ray laser. *Science (American Association for the Advancement of Science)*, *361*(6398), eaat0094. doi:10.1126/science.aat0094

23. Otto, H., Marti, T., Holz, M., Mogi, T., Stern, L. J., Engel, F., ... &Heyn, M. P. (1990). Substitution of amino acids Asp-85, Asp-212, and Arg-82 in bacteriorhodopsin affects the proton release phase of the pump and the pK of the Schiff base. *Proceedings of the National Academy of Sciences*, *87*(3), 1018-1022.

24. Luecke, H., Schobert, B., Richter, H., Cartailler, J., &Lanyi, J. K. (1999). Structure ofbacteriorhodopsin at 1.55 Å resolution. *Journal of Molecular Biology*, *291*(4), 899-911. doi:10.1006/jmbi.1999.3027

25. Thavasi, V., Lazarova, T., Filipek, S., Kolinski, M., Querol, E., Kumar, A., Renugopalakrishnan, V. (Mar 2009). Study on the feasibility of bacteriorhodopsin as bio-

photosensitizer in excitonic solar cell: A first report. Paper presented at the Retrieved from http://scholarbank.nus.edu.sg/handle/10635/86086

26. Mohammadpour, R., &Janfaza, S. (2015). Efficient nanostructured biophotovoltaic cell based on bacteriorhodopsin as biophotosensitizer. *ACS Sustainable Chemistry & Engineering*, *3*(5), 809-813.

27. Das, S., Wu, C., Song, Z., Hou, Y., Koch, R., Somasundaran, P., ... & Venkatesan, R. (2019). Bacteriorhodopsin enhances efficiency of perovskite solar cells. *ACS applied materials &interfaces*, *11*(34), 30728-30734.

28. Naseri, N., Janfaza, S., & Irani, R. (2015). Visible light switchable bR/TiO 2 nanostructured photoanodes for bio-inspired solar energy conversion. *RSC Advances*, *5*(24), 18642-18646. doi: 10.1039/c4ra16188b

29. Allam, N., Yen, C., Near, R., & El-Sayed, M. (2011). Bacteriorhodopsin/TiO2 nanotube arrays hybrid system for enhanced photoelectrochemical water splitting. *Energy & Environmental Science*, *4*(8), 2909. doi: 10.1039/c1ee01447a

30. Li, Y., Tian, Y., Tian, H., Tu, T., Gou, G., Wang, Q., . . . Ren, T. (2018). A review on bacteriorhodopsin-based bioelectronic devices. *Sensors (Basel, Switzerland), 18*(5), 1368. doi:10.3390/s18051368

31. Ostrovsky, M. A., &Kirpichnikov, M. P. (2019). Prospects of optogenetic prosthesis of the degenerative retina of the eye. *Biochemistry (Moscow)*, *84*(5), 479-490

32. N.L Wagner, R.R Birge "Visual Restoration Using Microbial Rhodopsin. In Bionanotechnology: Biological Self-Assembly and Its Applications" Bio nanotechnology: Biological Self- Assembly and Its Applications, B. H. A." Rehm, ed. Caister Academic Press, Norfolk, United Kingdom, pp. 205-240, 2013

33. Sz. Tőkés, T. Roska "Bacteriorhodopsin as An Analog Holographic Memory for Joint Fourier Implementation of CNN Computers" Research Report DNS-3-2000.

34. Birge, R. R., Gillespie, N. B., Izaguirre, E. W., Kusnetzow, A., Lawrence, A. F., Singh, D., ... & Wise,K. J. (1999). Biomolecular electronics: protein-based associative processors and volumetric memories.

35. E. T. Castellana and Paul S. Cremer "Solid supported lipid bilayers: From biophysical studies to sensor design", Surface Science Reports, Vol. 61, pp. 429–444, 2006

36. Membranes and Membrane Lipids. (2021). Retrieved 7 January 2021, From https://saylordotorg.github.io/text_the-basics-of-general-organic-and-biological-chemistry/s20-03-membranes-and-membrane-lipids.html

37. P. Muller, H. Ti Tien, W.C. Wescott, "Methods for Formation of Single Bimolecular Lipid

Membranes in Aqueous Solution" Journal of Physical Chemistry Vol.6, 1963 7, pp. 534535
38. L.K. Tamm and H.M. McConnell, "Supported Phospholipid Bilayers" Biophysics Journal Vol. 47, 1985, pp 105-113

39. S.G. Boxer, J.T. Groves, N. Ulman, "Micropatterning Fluid Lipid Bilayers on Solid Supports",ScienceVol. 651, 1997, pp 651-653

40. J. Spinke, J. Yang, "Polymer-Supported Bilayer on a Solid Substrate" Biophysics Journal, Vol. 63, 1992, pp. 1667-1671

41. Tristram-Nagle, S., Kim, D., Akhunzada, N., Kučerka, N., Mathai, J., &Katsaras, J. et al. (2010). Structure and water permeability of fully hydrated diphytanoylPC. *Chemistry And Physics Of Lipids, 163*(6), 630-637. doi: 10.1016/j.chemphyslip.2010.04.011

42. W. Shinoda, S. Mikami, M. Baba, T. Hato, "Molecular Dynamics Study on the Effects of Chain Branching on the Physical Properties of Lipid Bilayers" J. Phys. Chem. B Vol.108, 2004, pp. 9346–9356

43. L. P. Hromada, Jr. "Bilayer Lipid Membrane (BLM) Integration into Microfluidic Platforms with Application Toward BLM-based Biosensors" University of Maryland, College Park, 2007.

44. Kamwa, J. (2014). Photoelectric Characterization of Bacteriorhodopsin Reconstituted in Lipid Bilayer Membrane.

45. *Digidata ® 1440A low-noise data acquisition system user guide* (2010)

46. The Axon™ Guide A guide to Electrophysiology and Biophysics Laboratory Techniques 1-2500-0102 D.

47. http://www.moleculardevices.com/Products/Instruments/Conventional-PatchClamp/Axon-Axopatch.htm .

48. http://www.chemistryrules.me.uk/tandp/optiontransitionelements.htm (accessed on 09/21/2014)

49. pCLAMP 10 Data Acquisition and Analysis for Comprehensive Electrophysiology User Guide 1-25000180 Rev. A

50. Beckman Coulter, I. DU 800 Spectrophotometer Installation and Operating Instructions. 2009 Nov, 2009 Jan 10, 2017

51. Wydro, P., Flasiński, M., &Broniatowski, M. (2012). Molecular organization of bacterial membrane lipids in mixed systems—A comprehensive monolayer study combined with Grazing Incidence X-ray Diffraction and Brewster Angle Microscopy experiments. *Biochimica et Biophysica Acta (BBA)-Biomembranes, 1818*(7), 1745-1754.

52. Sigma-Aldrich 3050 Spruce St. St. Louis, MO 63103

53. TCI America 9211 North Harborgate Street Portland, OR 97203 45.

54. J.T.BAKER INC., 222 Red School Lane, Phillipsburg, NJ 08865

55. C. Horn and C. Steinem "Photocurrents Generated by Bacteriorhodopsin Adsorbed on Nano-Black Lipid Membranes", Biophysical Journal, Vol. 89, pp. 1046–1054, 2005

56. Ormos, P., Hristova, S., &Keszthelyi, L. (1985). The effect of pH on proton transport by bacteriorhodopsin. *Biochimica et Biophysica Acta (BBA)-Bioenergetics*, *809*(2), 181-186

57. M.Takagi, K. Azuma, U. Kishimoto, "A new method for the formation of bilayer membranes in aqueous solution" Annual Report Biology Osaka University Vol. 13, pp. 107-110, 196558. M. Montal and P. Mueller "Formation of Bimolecular Membranes from Lipid Monolayers and a Study of Their Electrical Properties" Proc. Nat. Acad. Sci. USA, Vol. 69, 1972, pp. 3561-3566

59. L. P. Hromada, Jr. "Bilayer Lipid Membrane (BLM) Integration into Microfluidic Platforms with Application Toward BLM-based Biosensors" University of Maryland, College Park, 2007.

60. Jin, Y., Honig, T., Ron, I., Friedman, N., Sheves, M., &Cahen, D. (2008). Bacteriorhodopsin as an electronic conduction medium for biomolecular electronics. *Chemical Society Reviews*, *37*(11), 2422-2432

61. El-Beyrouthy, J., & Freeman, E. (2021). Characterizing the Structure and Interactions of Model Lipid Membranes Using Electrophysiology. *Membranes*, *11*(5), 319.

62. Wang, L. (2012). Measurements and implications of the membrane dipole potential. *Annual review of biochemistry*, *81*, 615-635.

63. Zhan, H., & Lazaridis, T. (2012). Influence of the membrane dipole potential on peptide binding to lipid bilayers. *Biophysical chemistry*, *161*, 1-7.

64. Antonov, V. F., Petrov, V. V., Molnar, A. A., Predvoditelev, D. A., & Ivanov, A. S. (1980). The appearance of single-ion channels in unmodified lipid bilayer membranes at the phase transition temperature. *Nature*, *283*(5747), 585-586.

65. Golowasch, J., Thomas, G., Taylor, A. L., Patel, A., Pineda, A., Khalil, C., & Nadim, F. (2009). Membrane capacitance measurements revisited: dependence of capacitance value on measurementmethod in nonisopotential neurons. *Journal of neurophysiology*, *102*(4), 2161-2175.

66. Lu, Z., Wang, J., Li, R., Qiao, Y., Zhou, M., & Li, C. M. (2016). Controllable stationary photocurrents generated from a bacteriorhodopsin/upconversion nanoparticle-based

bionanosystem under NIR illumination. *Nanoscale*, *8*(43), 18524-18530.

67. Al-Aribe, K. M., Knopf, G. K., &Bassi, A. S. (2015, December). Ionic polymer microactuator activated by photoresponsive organic proton pumps. In *Actuators* (Vol. 4, No. 4, pp. 237-254). Multidisciplinary Digital Publishing Institute.

68. Horn, C., & Steinem, C. (2005). Photocurrents generated by bacteriorhodopsin adsorbed on nano-black lipid membranes. *Biophysical journal*, *89*(2), 1046-1054

69. T. R. Hermann and G. W. Rayfield "A measurement of the proton pump current generated by Bacteriorhodopsin in black lipid membranes" Biochimica et Biophysica Acta, 443, pp. 623-628, 1976